LA-6560-PR
Progress Report

Special Distribution
Issued: November 1976

Applied Nuclear Data Research and Development

April 1—June 30, 1976

Compiled by

C. I. Baxman
P. G. Young

los alamos
scientific laboratory
of the University of California
LOS ALAMOS, NEW MEXICO 87545

An Affirmative Action/Equal Opportunity Employer

UNITED STATES
ENERGY RESEARCH AND DEVELOPMENT ADMINISTRATION
CONTRACT W-7405-ENG. 36

The four most recent reports in this series, unclassified, are LA-6472-PR, LA-6266-PR, LA-6164-PR, and LA-6123-PR.

This work was performed under the auspices of the Defense Nuclear Agency, the Nuclear Regulatory Commission, the National Aeronautics and Space Administration, and the US Energy Research and Development Administration's Divisions of Military Application, Reactor Development and Demonstration, Physical Research, and Magnetic Fusion Energy.

CONTENTS

APPLIED NUCLEAR DATA RESEARCH AND DEVELOPMENT
QUARTERLY PROGRESS REPORT
April 1 - June 30, 1976

Compiled by

C. I. Baxman and P. G. Young

ABSTRACT

This progress report describes the activities of the Los Alamos Nuclear Data Group for the period April 1 through June 30, 1976. The topical content is summarized in the contents.

I. THEORY AND EVALUATION OF NUCLEAR CROSS SECTIONS

A. R-Matrix Analysis of Reactions in Light Systems (G. M. Hale and D. Dodder [T-9])

Our program of analyzing reactions in light systems using multichannel R-matrix theory has generally overlapped two areas of applied interest, light-element standards and fusion reactions. In this quarter we have extended and modified analyses of the ^{7}Li and ^{11}B systems which were substantially completed last quarter to provide standard cross sections for Version V of the Evaluated Nuclear Data File (ENDF/B), and have restarted analysis of the 4 and 5 nucleon systems which contain many of the important fusion reactions.

1. Standards. New data have been added to the ^{7}Li analysis which was used to provide evaluated ^{6}Li(n,α) cross sections at low energies for Version V. These include α-t cross section excitations[1] measured over the resonance which occurs at ~250-keV neutron energy, and measurements of the ^{6}Li(n,t) angular distributions[2] at energies above 2 MeV. The new data are fitted quite well with only slight changes in the R-matrix parameters, indicating, for instance, a preference for the integrated ^{6}Li(n,α) cross section values of Bartle[2] over those of Clements and Rickard[3] at neutron energies above 2 MeV. These results were reported at the International Conference on the Interaction of Neutrons with Nuclei at Lowell, Massachusetts.

Modifications in the analysis of reactions in the ^{11}B system were required to reflect changes in the preliminary $^{10}B(n,\alpha\gamma)$ cross section data[4] measured at the National Bureau of Standards which had strongly influenced the calculated $^{10}B(n,\alpha)$ cross sections proposed for use as Version V standards. These changes, which are significant only at energies above 500 keV, will be incorporated in the final ENDF/B-V file.

2. Fusion Reactions. We have incorporated new data in our comprehensive analysis of both the ^{5}He and ^{5}Li systems. In the case of ^{5}Li, the changes in data base have been extensive, since earlier $^{3}He(d,d)^{3}He$ measurements of Konig[5] have been supplanted by the newer, more complete measurements of Jenny.[6] In addition, the vector analyzing power measurements of Klinger[7] for the $^{3}He(\vec{d},p)^{4}He$ reaction have been included, as well as data in all reactions at higher energies. Our hope is that these new measurements are sufficiently reliable to sort out at last the complicated sequence of overlapping d-wave (and possible odd-parity) levels which exist in the 5-nucleon system above the well-known $3/2^{+}$ S-wave resonance. New data have been accommodated in the ^{5}He system analysis, including measurements of the T(d,d)T vector analyzing power[8] and precision values of the $T(d,n)^{4}He$ cross sections.[9] with little change in the R-matrix parameters.

A new charge-independent analysis of reactions in the ^{4}He system has begun, which will soon extend to energies above the d + d threshold. One of the goals of this analysis is to obtain R-matrix fits to the D(d,p)T and $D(d,n)^{3}He$ cross sections which have reliable extrapolations to zero deuteron energy, as has already been done for the $T(d,n)^{4}He$ and $^{3}He(d,p)^{4}He$ cross sections using analyses like those described above.

B. Calculations of (n,xn) Cross Sections and Spectra (E. D. Arthur, P. G. Young, and L. R. Veeser [P-3])

We have completed calculations of cross sections and spectra for (n,xn) reactions on ^{45}Sc, ^{58}Ni, ^{59}Co, ^{89}Y, ^{93}Nb, ^{103}Rh, ^{169}Tm, ^{175}Lu, ^{181}Ta, ^{197}Au, and ^{209}Bi. For these calculations we used the preequilibrium-statistical model code GNASH with global optical model and level density parameters with no attempt to adjust parameters to better fit experimental data. The calculated spectra of first and second neutrons from (n,2n) events and the spectra for first, second, and third neutrons from (n,3n) events were used by Veeser and Arthur[10] to make efficiency corrections to measurements made with a large liquid scintillator tank.

Comparisons of the calculated cross sections to recent (n,xn) measurements of Frehaut and Mosinski,[11] Bayhurst et al.,[12] and Veeser et al.[10] were made in a paper presented at the 1976 International Conference on the Interactions of Neutrons with Nuclei. Selected examples of the agreement of calculated to experimental results are shown in Figs. 1-3 for (n,xn) reactions on ^{89}Y, ^{181}Ta, and ^{209}Bi. In order to fit the experimental (n,2n) and (n,3n) cross sections at higher energies, it was necessary to include contributions from preequilibrium processes. For example, the long dashed curve in Fig. 4 illustrates cross sections calculated without preequilibrium effects. Also important is the mass and energy dependence of the absolute square of the average effective matrix element M of residual two-body interactions, which appear in the expressions used to calculate the preequilibrium component. In Fig. 4 the short dashed curve illustrates results obtained when preequilibrium effects are included with the quantity

$$|M|^2 \alpha\ A^{-3} \quad ,$$

as suggested by Braga-Marcazzan et al.[13] Finally, the solid curve (as well as the curves in Figs. 1-3) shows the result obtained when the preequilibrium component is included with a mass and excitation energy dependence

$$|M|^2 \alpha\ A^{-3} E^{-1} \quad ,$$

as determined by Kalbach-Cline.[14]

As a result of this work, we feel that calculations which include preequilibrium effects and which use global input parameters can reproduce well the experimental data for (n,xn) reactions.

C. Calculations of Charged-Particle Spectra Induced by 15.1-MeV Neutrons

E. D. Arthur and P. G. Young

We have made further calculations of the charged-particle production spectra from 15.1-MeV neutron bombardment of ^{27}Al, ^{46}Ti, and ^{48}Ti to compare with the most recent measurements of Grimes et al.[15] These calculations are an extension of earlier calculations made with the GNASH preequilibrium-statistical model code with global optical model and level density parameters. Preequilibrium effects, which are important in reproducing the observed spectral shapes and cross section

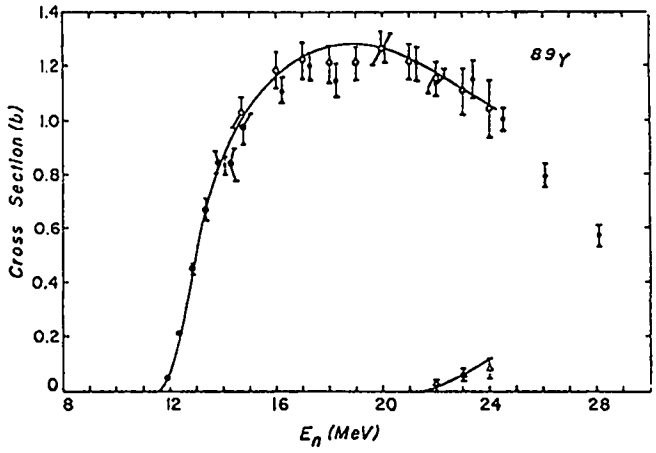

Fig. 1.
Comparison of calculations and experiment for $^{89}Y(n,xn)$ reactions to the data of Frehaut,[11] Veeser,[10] and Bayhurst.[12]

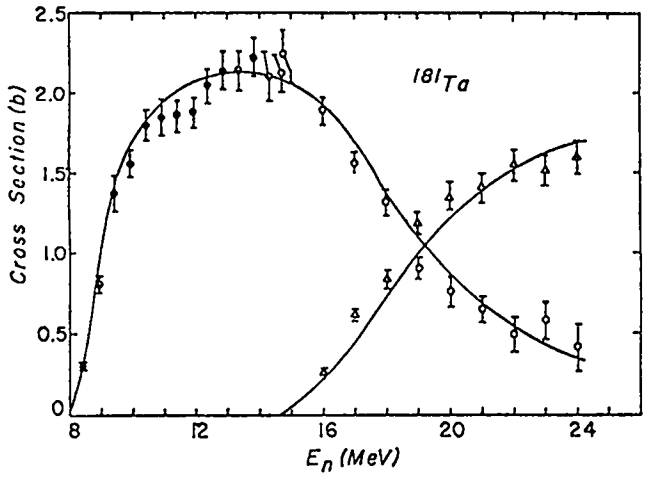

Fig. 2.
The calculations for $^{181}Ta(n,xn)$ reactions are compared with the measurements of Frehaut[11] and Veeser.[10]

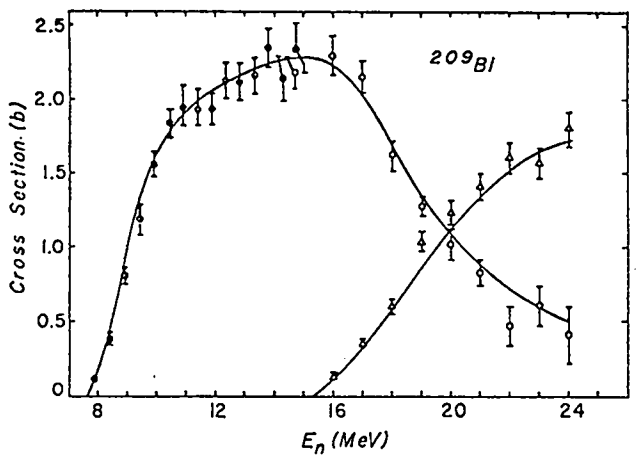

Fig. 3.
The calculations for ^{209}Bi reactions are compared with the measurements of Frehaut[11] and Veeser.[10]

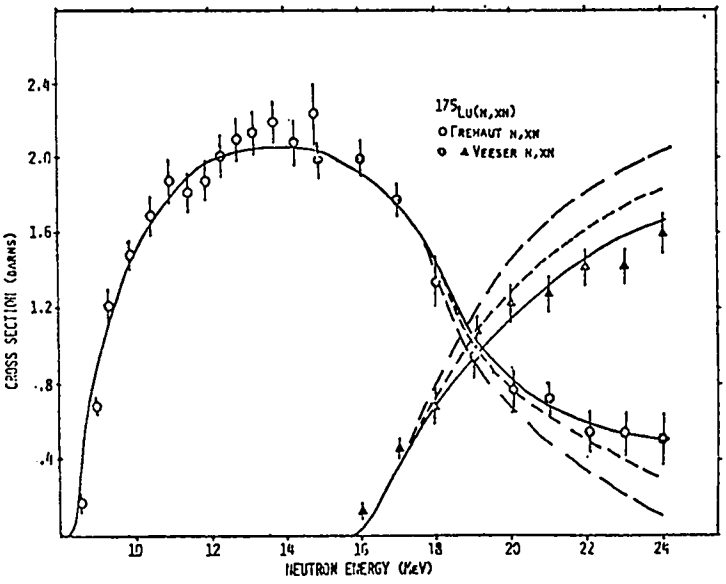

Fig. 4.
Calculations of $^{175}Lu(n,xn)$ reactions are compared to the data of Frehaut and Veeser. The - - curve was made with no preequilibrium effects, the --- curve included a preequilibrium component whose normalization depended on mass, while the solid curve was made with a preequilibrium component normalized to both mass and excitation energy.

magnitudes, were made using the closed form exciton expression of Milazzo-Colli et al.[16] The preequilibrium component was assumed to be normalized such that

$$|M|^2 \alpha\ A^{-3}E^{-1} \quad ,$$

where M is the matrix element describing residual two body interactions. The absolute normalization was obtained from a survey of experimental (n,n'), (n,p), and (n,α) results.

Comparisons with the data of Grimes et al.[15] for proton production from ^{46}Ti and ^{48}Ti are shown in Fig. 5. The calculations reproduce well the striking difference in the spectrum of protons from these two isotopes. In Fig. 6, comparisons of the calculations are made with the ^{46}Ti deuteron and alpha production data. Except for the ^{46}Ti(n,d) reaction, no attempt was made to adjust parameters to improve the fit to experimental data. In the case of the (n,d) data, direct reaction effects, which are not included explicitly in these calculations, may account for some of the disagreement between the calculations and experiment.

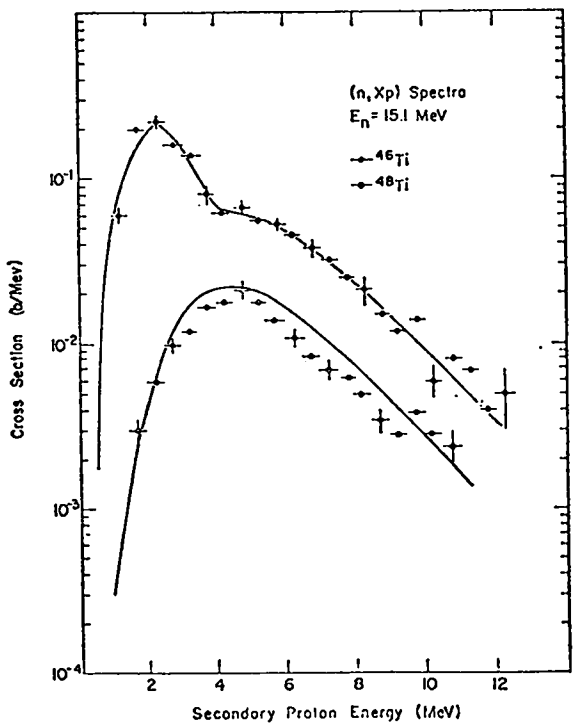

Fig. 5.
A comparison between calculated and experimental results for the proton production spectra from ^{46}Ti and ^{48}Ti.

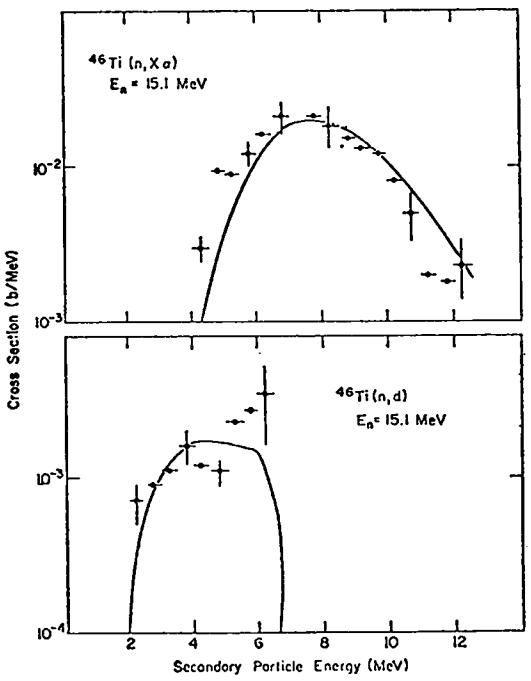

Fig. 6.
A similar comparison for ^{46}Ti alpha and deuteron production spectra.

D. Fast Fission Cross Sections (L. Stewart)

Several recommendations were made at the NEANDC/NEACRP Specialists Meeting on Fast Neutron Fission Cross Sections held at Argonne National Laboratory on June 28-30. The most important, perhaps, were the agreement on the method of shifting energy scales and the normalization of the 28/25 fission ratio measurements. Above 10-MeV incident neutron energy, however, several problems remain. The disagreement among the experiments on the 49/25 ratios is not yet understood, even at 1 MeV.

A paper entitled, "What Happens to the Fission Process Above the 2nd and 3rd Chance Fission Thresholds?" by Leona Stewart and Robert Howerton, was presented at this meeting.

E. Neutron Spectra From Fission (L. Stewart)

All of the fissile and fertile materials on ENDF/B, except ^{233}U, have a Maxwellian representation for the fission neutron spectrum. Recent experiments indicate somewhat better agreement with a Watt distribution rather than the Maxwellian used in Version IV. A format to allow an energy-dependent Watt spectrum was recently approved by the Cross Section Evaluation Working Group (CSEWG), and the spectra for some of the important isotopes will be updated accordingly for Version V. A paper on this subject entitled, "The Prompt-Neutron Fission Spectrum for ^{239}Pu," by E. Kujawski (General Electric, Sunnyvale) and L. Stewart has been accepted for presentation at the American Nuclear Society Winter Meeting.

While the Watt spectrum is quite reasonable, some of the recent measurements have shown far too many low-energy neutrons (<1 MeV) to agree with earlier experiments or with the Watt or the Maxwellian distribution. This problem is still to be resolved and it is hoped that some explanation will be found in the experiments. An additional problem is that almost nothing is known about the incident neutron energy dependence of the fission neutron spectrum. It is expected that essentially the same average fission neutron energy used in Version IV will be implemented in Version V with the above change in shape.

F. Evaluated Time-Dependent Photon Spectra From a ^{235}U Fission Burst (D. G. Foster, Jr., T. R. England, and M. G. Stamatelatos)

A preliminary evaluation of the time-dependence of the intensity and spectrum of photons emitted following a very short fission burst (<<1 ns) was

completed[17,18] a year ago. It covered fission induced by thermal neutrons in ^{235}U and ^{239}Pu. Special attention had been devoted to the time range less than 1 s after fission, but only a crude extrapolation to 10^8 s was included. This extrapolation assumed a time-independent spectrum after 60 s, and used old data normalized to recent data at 15 s, where the log-log slopes of the 2 sets of data were equal.

We have now replaced the data for ^{235}U at times greater than 15 s with detailed calculations using ENDF/B-IV data in the CINDER code. The input data cover 825 fission-product nuclides, but only 181 of these (selected to account for most of the energy emitted at decay times greater than a few seconds) have spectral information. The overall spectrum is assumed to be that of these 181 nuclides. The calculations were made using an irradiation time of 10^{-4} s, so that the results are indistinguishable from an arbitrarily short burst at decay times greater than a second. The calculated absolute yield joins neatly onto the results of Fisher and Engle[19] at 50 s after fission, and is thus about a factor of 3 lower than the previous extrapolation at 60 s, as pointed out a year ago.[18] The new intensity is roughly equal to the previous intensity between 10^5 and 10^7 s, but is a factor of 10 lower at 10^8 s. The new evaluation has also been extended to 10^9 (31.7 y). The accuracy from 50 s to a few hours appears to be ± a few percent.

The spectrum in the new evaluation displays a marked variation with time. The average photon energy has 5 pronounced minima between 1 and 10^9 s, with an overall range from 0.43 to 1.05 MeV. This is in sharp contrast to the constant spectrum assumed in the previous evaluation.

We are currently working on the CINDER calculations for neutron-induced fission of ^{239}Pu. We expect to submit the completed work on both isotopes for possible inclusion in ENDF/B-V.

G. Computation of Specific Thermonuclear Reaction Rates--The STEEP Code (D. E. Dei [Carnegie Mellon University], A. A. Husseiny [Iowa State University] and G. M. Hale)

A fast, efficient, and accurate program module, STEEP, has been developed to compute specific thermonuclear reaction rates, $\langle\sigma v\rangle$. These quantities are central in the design and analysis of various fusion devices, as well as other areas (e.g., astrophysical problems). Because of this wide range of potential applicability, STEEP is designed for a variety of plasma conditions.

The most common reaction rate computations involve the interaction of ion distributions in Maxwellian equilibrium. In this case the specific reaction rate is written as a single integral over relative energy, E_r,[20]

$$\langle\sigma v\rangle_M = \int_0^\infty dE_r M_T(E_r)\sigma(E_r)v_r(E_r) \quad , \tag{1}$$

where M_T is a Maxwellian distribution in energy. For accurate but rapid results Eq. (1) is integrated numerically with a self-terminating trapezodial quadrature. Values of $\sigma(E_r)$ are effectively supplied from an evaluated library of energy-cross-section pairs (e.g., from R-matrix calculations) with suitable interpolation formula provided to evaluate $\sigma(E_r)$ for arbitrary energies.

In many instances, the plasma ions are not in thermal equilibrium and a sizeable contribution to the reaction rate is produced by a high energy slowing down component of the distributions. For this case STEEP assumes a continuous slowing down model wherein leakage and absorption are neglected and the confinement time is assumed to be greater than the slowing down time, τ_{SD}. The slowing down component of the i-th ion distribution, with source strength S_0 below the source energy E_0 is

$$n_{SD}(E_i) = \frac{S_0}{\langle dE_i/dt\rangle} \quad . \tag{2}$$

When the total ion density N_i is known, n_{SD} is joined to a background Maxwellian component so that

$$n(E_i) = \begin{cases} N_i\ (1-a_i)\ M_T(E_i) \ , & E_i < E_m \text{ and } E_i > E_0 \ , \\ N_i\ \{(1-a_i)\ M_T(E_i) + \dfrac{a_i}{\langle dE_i/dt\rangle\ \tau_{SD}}\} \ , & E_m \leq E_i \leq E_0 \ . \end{cases} \tag{3}$$

E_m is a lower cutoff, usually taken as 2kT, and a_i is given by $S_0\tau_{SD}/N_i$. The total specific reaction rate is

$$\langle\sigma v\rangle = (1-a_i)\ \langle\sigma v\rangle_M + \langle\sigma v\rangle_{SD} \quad , \tag{4}$$

where

$$\langle\sigma v\rangle_{SD} = \frac{2S_0}{N_i}\left(\frac{m_j}{2\pi kT}\right)^{\frac{1}{2}}\int_{E_m}^{E_0}\frac{dE_i}{v_i\langle dE_i/dt\rangle}\int_0^{\infty}dv_r\, v_r^2\,\sigma(v_r)\,\frac{\sinh\left(\frac{m_j v_r v_i}{kT}\right)}{\exp\left(\frac{m_j(v_r^2+v_i^2)}{2kT}\right)} \quad . \quad (5)$$

In two-component fusion devices,[21] a primary design parameter is the energy multiplication factor F, which is related to $\langle\sigma v\rangle_{SD}$ by

$$F = \frac{Q_{ij}}{S_0E_0} N_iN_j \langle\sigma v\rangle_{SD} \quad , \quad (6)$$

where Q_{ij} is the energy release per fusion event.

Figure 7 shows typical results obtained with STEEP for the D-T, D-^{3}He, and p-^{11}B fusion reactions. D-T and D-^{3}He cross sections were obtained from an R-matrix analysis[22] which considered the T(d,n) and ^{3}He(d,p) reactions simultaneously in a charge-independent framework. The p-^{11}B cross section was provided by a premliminary R-matrix evaluation.[23] The low temperature $\langle\sigma v\rangle_M$ values are generally higher (10-20%) than previous results[24-26] due to improved low energy cross sections. Also, Hale's larger D-^{3}He cross section results in 10-15% increases over previous results[24-27] in both $\langle\sigma v\rangle_M$ and F-factors for the D-^{3}He fuel system. Previous results suggest that the two-component D-^{3}He scheme, while having highly attractive features such as lack of neutron and tritium production, is only marginally capable of near-future breakeven. In this light, our results for D-^{3}He are of particular interest and indicate the need for continued study of this system.

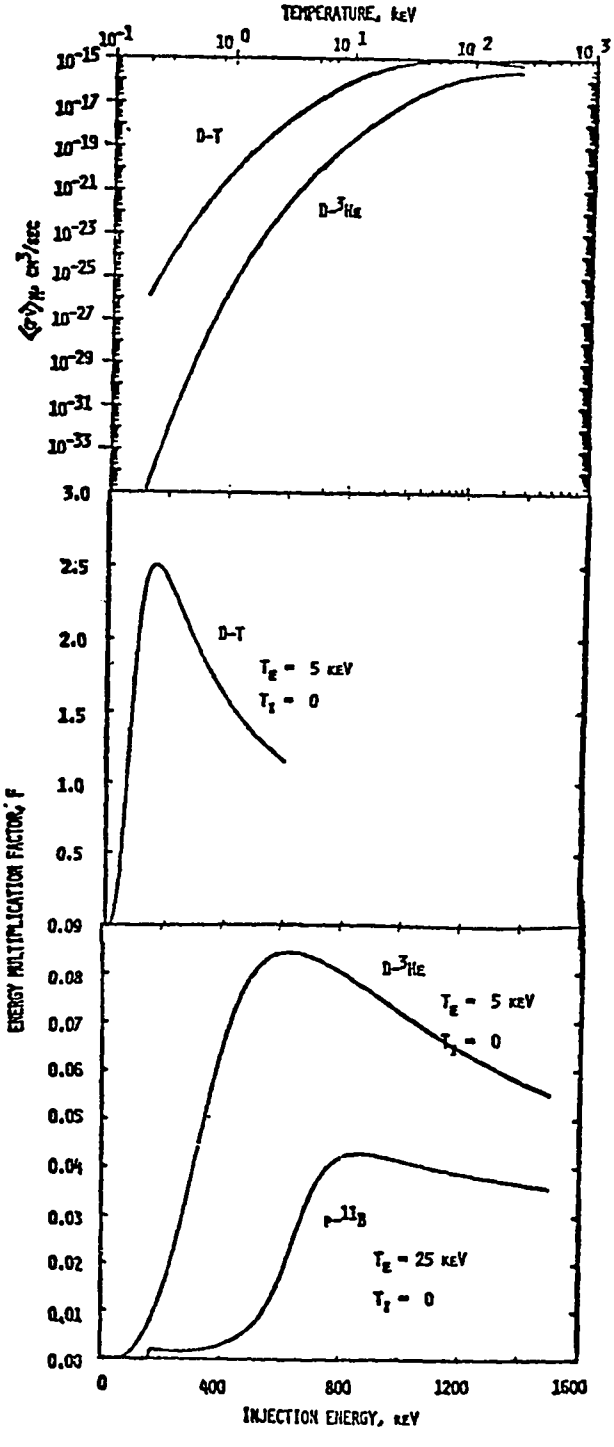

Fig. 7.
Maxwellian-averaged specific reaction rate $\langle\sigma v\rangle_M$ and two-component energy multiplication factor F for D-T, D-^{3}He, and p-^{11}B fusion reactions.

II. NUCLEAR CROSS-SECTION PROCESSING

A. Neutron Photon Coupled Sets from ENDF/B-IV (D. W. Muir and R. E MacFarlane)

During this quarter we have used NJOY to produce multigroup cross section sets for the following materials--^{1}H, ^{2}H, ^{3}H, ^{3}He, ^{4}He, ^{6}Li, ^{7}Li, ^{10}B, ^{11}B, ^{12}C, ^{14}N, ^{16}O, ^{19}F, ^{27}Al, Si, ^{55}Mn, Mo, ^{197}Au, Pb, ^{233}U, ^{241}Pu, and ^{242}Pu. These calculations utilize 0° pointwise cross sections from the T-2 PENDF library.[28] P_0 through P_4 neutron transport tables were prepared in the TD-Division format using basic data from ENDF/B-IV. For all materials except ^{11}B, ^{197}Au, and the fissionable isotopes listed above, 30 x 12 gamma-ray production matrices and 12-group gamma-ray interaction cross sections[29] were also prepared. Gamma-ray production evaluations are not given in ENDF/B-IV for ^{3}H, ^{3}He, and ^{4}He, but the production cross sections should be very small or zero for all 3 isotopes. Thus we have entered zeros in the gamma-ray production matrices for these isotopes. For all of the gamma materials (including ^{3}H, ^{3}He, and ^{4}He), neutron/gamma coupled sets were then prepared using PROSEC.[30]

The coupled sets were written, along with the usual TD-format edit cross sections and uncoupled cross sections, to HYDRA photostore files (OAC = TO2DWM). As before, file marks separate the three data types and the usual naming convention is followed (H1MG, H2MG, ..., S1MG, MN55MG, MOMG, ..., PU242MG). The five materials for which gamma information is absent are written in the older form (i.e., without internal file marks). The special T-2 evaluations for ^{6}Li and ^{12}C (Ref. 31) also have been processed. These evaluations treat the continuum breakup reactions $^{6}Li(n,n'd\alpha)$ and $^{12}C(n,n'3\alpha)$ with the pseudo-level formalism. The output files for these materials are on photostore files LI6AMG and C12AMG, respectively, in coupled-set format.

B. Pointwise Cross-Section Library for MCNG (R. J. LaBauve and D. George)

Over the past year and a half, T-2 has participated in supplying data for the TD-6 continuous energy Monte Carlo library.[31] Thus far, data have been provided for 57-nuclide temperature combinations as shown in Table I. All materials shown in the table contain photon-production data (MF=13,14,15) as well as neutron data. Materials with 7000-series MAT numbers were taken from the Lawrence Livermore Laboratory's (LLL) evaluated nuclear data file (ENDL). MAT numbers 101 and 102 are local T-2 evaluations, and all others are taken from ENDF/B-IV.

Several different processing routes were followed in going from the original data files to the photostore files given in the table.

TABLE I

MATERIALS IN PENDF LIBRARY

MAT	TARGET	PHOTOSTORE FILE NAME	TEMPERATURE	MF=4 THIN TOLERANCE (PERCENT)	MF=3 LIN TOLERANCE (PERCENT)	MF=3 THIN TOLERANCE (PERCENT)	PHOTOSTORE FILE LENGTH (WORDS)	MAX NO. POINTS PER REACTION (MF=3)
101	3-LI-6	M101A	0.	3.	10.000	.100	40157	399
102	6-C -12	M102B	0.	10.	10.000	.100	37622	442
1120	1-H -2	M1120A	0.	3.	10.000	.100	17497	195
1129	74-W -182	M1128C	0.	3.	.001	.001	95323	4186
1129	74-W -183	M1129A	0.	3.	.001	.001	84183	3221
1130	74-W -184	M1130A	0.	3.	.001	.001	83051	3363
1131	74-W -186	M1131A	0.	3.	.001	.001	90013	3773
1190	28-NI	M1190AB	3.00E+02	10.	.001	.001	105109	3981
1190	28-NI	M1190BD	9.00E+02	10.	.001	.001	118132	4871
1191	24-CR	M1191CB	3.00E+02	10.	.001	.001	128139	3429
1191	24-CR	M1191CD	9.00E+02	10.	.001	.001	163811	4993
1192	26-FE	M1192AB	3.00E+02	10.	.001	.001	173358	4856
1192	26-FE	M1192D	9.00E+02	10.	.001	.001	185571	4903
1193	13-AL-27	M1193A	0.	3.	10.000	.100	138778	2161
1195	20-CA	M1195A	0.	3.	.100	5.000	89693	1536
1196	23-V	M1196A	0.	3.	10.000	5.000	30480	559
1261	92-U -235	M1261AC	3.00E+03	3.	.001	.001	123371	2908
1261	92-U -235	M1261BD	3.00E+04	3.	.001	.001	91625	1549
1261	92-U -235	M1261BE	6.00E+04	3.	.001	.001	74306	836
1261	92-U -235	M1261BF	1.20E+06	3.	.001	.001	77361	676
1261	92-U -235	M1261BA	0.	3.	.001	.001	208489	4595
1261	92-U -235	M1261BB	3.00E+02	3.	.001	.001	158632	4418
1262	92-U -238	M1262BD	3.00E+04	3.	.001	.001	122239	3491
1262	92-U -238	M1262AE	6.00E+05	3.	.001	.001	86637	1699
1262	92-U -238	M1262CF	1.20E+06	3.	.001	.001	62355	652
1264	94-PU-239	M1264AC	3.00E+03	3.	.001	.001	151630	4246
1264	94-PU-239	M1264AD	3.00E+04	3.	.001	.001	107774	2347
1264	94-PU-239	M1264AE	6.00E+05	3.	.001	.001	73314	880
1264	94-PU-239	M1264BF	1.20E+06	3.	.001	.001	66653	583
1264	94-PU-239	M1264AA	0.	3.	.001	.001	153223	4429
1264	94-PU-239	M1264AB	3.00E+02	3.	.001	.001	134180	3611
1265	94-PU-240	M1265AC	9.00E+01	3.	.100	.010	139429	4830
1269	1-H -1	M1269A	0.	3.	10.000	.100	17057	198
1271	3-LI-6	M1271A	0.	3.	10.000	.100	28548	317
1272	3-LI-7	M1272A1	0.	3.	10.000	.100	22977	255
1273	5-B -10	M1273A	0.	3.	10.000	.100	50063	443
1274	6-C -12	M1274A	0.	3.	10.000	.100	46547	516
1274	6-C -12	M1274AA	0.	10.	10.000	.100	34609	518
1275	7-N -14	M1275A	0.	3.	10.000	.100	140210	1152
1275	7-N -14	M1275AA	0.	10.	10.000	.100	117291	1152
1276	8-O -16	M1276A	0.	3.	10.000	.100	123451	1316
1276	8-O -16	M1276AA	0.	10.	10.000	.100	102359	1316
1277	9-F	M1277A1	0.	3.	10.000	.100	90234	1294
1288	AR-AR	M1288A	0.	3.	.100	5.000	77871	1283
1295	29-CU	M1295A	0.	3.	.100	5.000	57467	1199
7106	3-LI-6	M7106A	0.	3.	10.000	5.000	20442	71
7112	6-C -12	M7112A	0.	3.	10.000	5.000	18739	49
7113	7-N -14	M7113A	0.	3.	10.000	5.000	28065	259
7114	8-O -16	M7114A	0.	3.	10.000	5.000	17617	218
7132	26-FE	M7132A	0.	3.	.100	2.000	75508	2557
7143	41-NB-93	M7143A	0.	3.	.100	.010	88500	3721
7163	79-AU-197	M7163A	0.	3.	.100	5.000	59530	2462
7165	90-TH-232	M7165A	0.	3.	.100	.001	88651	4132
7166	92-U -233	M7166A	0.	3.	.100	5.000	33385	708
7167	92-U -234	M7167A	0.	3.	.100	5.000	20012	58
7168	92-U -235	M7168A	0.	3.	10.000	5.000	58799	1892
7171	92-U -238	M7171A	0.	3.	10.000	5.000	55773	1539

1. Some ENDF/B evaluations do not contain resonance parameters; that is, the cross-section data are completely described in MF=3. Materials of this type type were first processed by the TD-6 code ZERO, which shifts threshold energies in the data files to make them consistent with given Q-values, and then by the T-2 versions of the TOFFIL and ETOPL codes.[32] Included in this category are MATS 101, 102, 1120, 1160, 1193, 1269, 1273, 1274, 1275, and 1276.

2. The ENDL evaluations (the 7000-series MATS) processed are given pointwise as described above, and are generally in the ENDF/B format except for slight differences. For example, ENDL omits all isotropic angular distributions for secondary neutrons whereas the LASL code assumes these to be expressed explicitly. Modifications to the ENDL evaluations to make them compatible with LASL codes were made by R. Seamon in TD-6. The modified data sets were then processed with ZERO and the T-2 versions of the TOFFIL and ETOPL codes.

3. The remaining materials are those containing resonance parameters that were first translated to pointwise data by the MINX[33] code. Data for several temperatures were produced for each material and only those data sets containing less than 5000 points per reaction were processed directly by the T-2 codes. Those containing more than 5000 points were first processed by the TD-6 version of the ETOPL code which has the capability of processing large data sets and thinning to less than 5000 points, but it does not contain the module for processing the photon production files. All these nuclides were checked with the ZERO code before final runs with the T-2 codes.

All data sets were carefully checked by TD-6 with the aid of the TD-6 checking codes[30] LOOK4, MYGOD, and COMPXS before being incorporated into the TD-6 Monte Carlo data library. Also, checks were made by generating multigroup cross sections from these data sets with the MARK and LAPHANO codes and comparing them with multigroup cross sections derived from the original data sets.

C. LIB-IV-240 (Two-Hundred and Forty Group Library) (R. B. Kidman)

LIB-IV-240 is a 240-group library that is being generated with MINX[33] from ENDF/B-IV data.[34] Last quarter the library was started and many of its characteristics were described. This quarter, several more isotopes were added to LIB-IV-240. The resulting 52-isotope library, shown in Table II, should be complete enough for most nuclear reactor calculations.

A new resonance-smoothed weighting flux was introduced in MINX. It is exactly like the old thermal-1/E-fission function except above 10 MeV where a 1/E-

TABLE II

LIB-IV-240 MATERIALS GENERATED WITH MINX FROM ENDF/B-IV

I	ISOTOPE	ENDF/B VER IV MAT NO	PENDF NAME * VER NO	PENDF TIMING (SEC)	ISOTXS AND BRKOXS NAME * VER NO	ISOTXS AND BRKOXS FROM PENDF (SEC)	SIGO SET*
1	H-1	1269	H1P 1	133	H1L 1	612	A
2	H-2	1120	H2P 1	95	H2L 1	395	A
3	H-3	1169	H3P 1	165	H3L 1	767	A
4	HE-3	1146	HE3P 1	102	HE3L 1	279	B
5	HE-4	1270	HE4P 1	118	HE4L 1	451	B
6	LI-6	1271	LI6P 1	157	LI6L 1	667	A
7	LI-7	1272	LI7P 1	159	LI7L 1	733	A
8	BE-9	1289	BE9P 3	516	BE9L 1	4363	A
9	B-10	1273	B10P 3	428	B10L 1	1095	C
10	B-11	1160	B11P 5	182	B11L 1	466	D
11	C-12	1274	C12P 4	156	C12L 1	420	E
12	N-14	1275	N14P 1	593	N14L 1	1257	A
13	O-16	1276	O16P 1	590	O16L 1	1096	E
14	NA-23	1156	NA23P 2	667	NA23L 1	981	E
15	AL-27	1193	AL27P 2	631	AL27L 1	1155	D
16	SI	1194	SIP 1	546	SIL 1	1159	B
17	CA	1195	CAP 1	542	CAL 1	1310	B
18	TI	1286	TIP 4	218	TIL 1	566	D
19	V	1196	VP 1	344	VL 1	568	D
20	CR	1191	CRP 3	1641	CRL 1	2123	E
21	MN-55	1197	MN55P 2	705	MN55L 1	803	D
22	FE	1192	FEP 3	1075	FEL 1	1762	E
23	CO-59	1199	CO59P 2	910	CO59L 1	1158	B
24	NI	1190	NIP 3	1251	NIL 1	1350	E
25	CU	1295	CUP 2	707	CUL 1	1266	D
26	NB-93	1189	NB93P 1	2975	NB93L 1	2179	D
27	MO	1287	MOP 4	532	MOL 1	900	D
28	CD	1281	CDP 1	839	CDL 1	877	B
29	CD-113	1282	CD113P 1	605	CD113L 1	770	B
30	EU-151	1290	EU151P 2	900	EU151L 1	913	D
31	EU-153	1290	EU153P 2	785	EU153L 1	958	D
32	GD	1030	GDP 1	378	GDL 1	609	D
33	TA-181	1285	TA181P 4	1092	TA181L 1	1678	B
34	W-182	1128	W182P 2	2023	W182L 1	1873	D
35	W-183	1129	W183P 2	1353	W183L 1	2140	D
36	W-184	1130	W184P 2	1352	W184L 1	1659	D
37	W-186	1131	W186P 2	1489	W186L 1	1726	D
38	AU-197	1283	AU197P 2	1685	AU197L 1	1542	D
39	PB	1288	PBP 2	641	PBL 1	1871	B
40	TH-232	1296	TH232P 2	3850	TH232L 1	1922	D
41	U-233	1260	U233P 5	531	U233L 1	661	B
42	U-234	1043	U234P 2	672	U234L 1	618	D
43	U-235	1261	U235P 2	2832	U235L 1	3212	B
44	U-236	1163	U236P 2	780	U236L 1	650	D
45	U-238	1262	U238P 13	6454	U238L 1	4152	B
46	NP-237	1263	NP237P 1	2085	NP237L 1	1346	D
47	PU-238	1050	PU238P 3	1043	PU238L 1	906	D
48	PU-239	1264	PU239P 2	3505	PU239L 1	3336	F
49	PU-240	1265	PU240P 2	6113	PU240L 1	3702	D
50	PU-241	1266	PU241P 4	544	PU241L 1	865	D
51	AM-241	1056	AM241P 4	540	AM241L 1	620	D
52	PU-242	1161	PU242P 4	664	PU242L 1	689	D
				58893		69176	

* THE SIGO SETS ARE (IN BARNS):

SET A = 1000, 100, 10, 1, .1, .01
SET B = 10000, 1000, 100, 10, 1, .1
SET C = 1000, 100, 10, 1
SET D = 100000, 10000, 1000, 100, 10, 1
SET E = 1000, 100, 10, 1, .1
SET F = 10000, 1000, 100, 10, 1

fusion peak-1/E portion has been added. Thus we now have 10^{-5} eV < [thermal], < 0.1 eV < [1/E], < 0.8208 MeV < [fission], < 10 MeV < [1/E], < 12.57 MeV < [fusion peak] < 15.57 MeV < [1/E] < 20 MeV. The intent is to make the high-energy group cross sections more appropriate for fusion calculations. The old spectrum was used to generate ^{1}H, ^{2}H, ^{3}H, ^{4}He, ^{6}Li, ^{7}Li, ^{9}Be, ^{10}B, ^{11}B, ^{12}C, ^{14}N, ^{16}O, ^{23}Na, Fe and ^{239}Pu. All of the other isotopes were generated with the new spectrum.

After some testing, LIB-IV-240 will be released and shipped to those expressing an interest.

D. NJOY Storage Allocation Package (R. E. MacFarlane and R. M. Boicourt)

Large processing codes such as MINX and NJOY make extreme demands on the storage capacity of a computer. It is, therefore, important to make efficient use of the available storage. This requirement leads to systems of *variable-dimensioning* where blocks of data are stored in a large container array at locations specified by pointers. In many codes (MINX is an example), pointers are computed directly by the code and remain static throughout a particular calculation. Such systems are simple and efficient, but they are inflexible for problems whose storage demands change continuously during execution. In such cases, a system becomes desirable that dynamically allocates and reallocates storage space.

During this quarter we have developed a dynamic storage allocation system for NJOY called STORAG which combines features of existing systems into a simple and compact utility package. The package uses the four calls described below.

STORAG (NWMAX, NIDMAX, A) -- initializes the package and allocates space for NWMAX words and NIDMAX different data identifiers in the container array A.

RESERV (ID, NW, ID, A) -- reserve NW words in A for the data type identified by ID. The identifier can be integer or Hollerith. If NW = -1, the routine reserves all available space and returns the number of words in NW. This routine always tries to reserve space at the top of the container array. If insufficient room is available, it repacks the storage, eliminating any areas not currently in use and tries to allocate space again. Note that data in core may move around, but only if necessary.

RELEAS (ID, NW, A) -- release all but NW words for the data set identified by ID. If NW = 0, the ID is inactivated. The option NW > 0 is very useful in conjunction with the NW = -1 option of RESERV to read in data sets whose length cannot be determined in advance.

FINDEX (ID, IP, A) -- If data may have moved after a call to RESERVE, it is necessary to use this routine to locate the desired data set at location IP in the container array.

This system has been implemented throughtout NJOY giving a great increase in flexibility with no detectable decrease in efficiency.

E. Processing Photon Cross Sections (R. J. Barrett and R. E. MacFarlane)

The ability to produce photon scattering cross sections and photon production yields was added to the NJOY processing system earlier this year. Near-term plans call for the release of a photon production and photon scattering library in CCCC format, although it is not yet clear whether the format will consist of a combination of ISOGXS and ISONGX or the MATXS format described below (Sec. II G). Before such a library can be released however, a great deal of work must be done to develop methods of using it. Primarily this means either that methods for handling gammas should be built into existing space-energy collapse codes, or that data calculated within these codes must be made available to a separate gamma processor. For the time being, we have chosen the second alternative, employing the logic depicted in Fig. 8.

Data needed from the space-energy collapse code includes resonance self-shielding factors, zone mixture specifications, fine and coarse neutron group bounds, fine-group neutron cross sections, and zone-averaged, fine-group neutron fluxes. The 1DX code has been modified and is now capable of outputting a file called PHOCAL containing all of the necessary information.

The coding necessary to process the photon cross sections is embodied in a program called NDULG (Fig. 9). It is designed to self-shield the photon production for each isotope; collapse the neutron scattering, photon scattering, and photon production cross sections; calculate macroscopic cross sections by zone; and produce a neutron-gamma coupled set in ISOTXS format. Although the code is completely written, it has not been debugged.

F. CCCC Development (R. E. MacFarlane and R. J. Barrett)

Group T-2 continued its involvement in maintaining and improving the CCCC data files. In June, a set of revised specifications for the BRKOXS file was submitted to R. D. O'Dell of LASL T-1 for inclusion in Version IV. Proposed revisions to Version III included an option to block the f-factor record by reactions, and a parameter which specifies the number of reactions present. These revisions allow the user to generate self-shielding factors for as many reactions

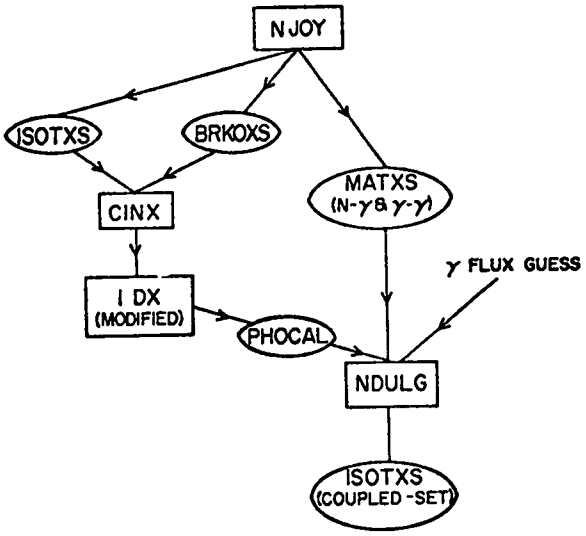

Fig. 8.
Calculational scheme for producing space-energy shielded neutron-gamma coupled sets.

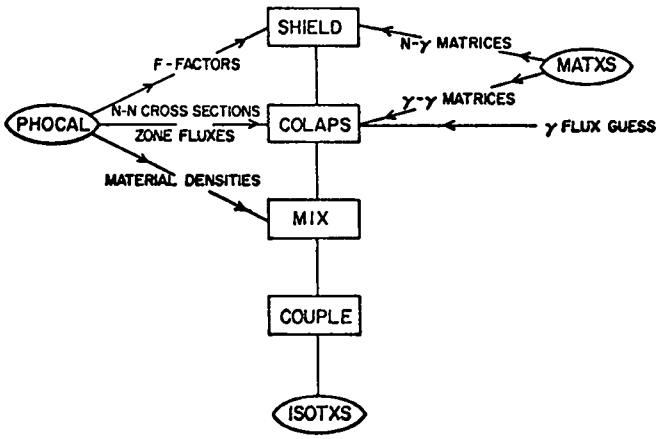

Fig. 9.
Block diagram of NDULG code.

as he chooses and for large group structures, without creating unmanageably large records. Both revisions have been included in the preliminary Version IV specifications, circulated on June 14, 1976.

G. Comprehensive CCCC Cross-Section File -- MATXS (R. J. Barrett and R. E. MacFarlane)

At the May 4-5 meeting of the Committee on Computer Code Coordination (CCCC), there was a great deal of discussion about the need for a comprehensive isotope-ordered cross-section file. C. R. Weisbin of Oak Ridge National Laboratory (ORNL) argued that the present cross-section files (ISOTXS, ISOGXS) were not flexible enough to handle neutron-gamma coupled sets. Furthermore, there was no provision for specifying whether the files contained microscopic or macroscopic data, or whether the data were cross sections or multiplicities (particle yields). General agreement was reached that a comprehensive file was needed which could encompass a wide variety of data, and which would have the type of flexibility discussed above. Specifications for a file called CCCCCF, developed by J. L. Lucius of ORNL, were distributed for perusal and comment. It was decided that the ORNL and LASL data groups, in conjunction with Westinghouse and General Electric, should work out a suitable file specification.

In studying the ORNL proposal, we uncovered a number of difficulties which we thought should be corrected.

1. The file was not similar enough to ISOTXS in the way it blocked and sub-blocked matrix data. We believed this would cause undue difficulties in converting existing codes and libraries to the new format.

2. It would be difficult to skip around within the file. For instance, within a given isotope, all vector cross sections for all types of data were together, followed by all matrix data; furthermore there were no location data (LOCA) for skipping isotopes or data types.

3. There were not enough descriptors to tell the user what type of data is present in a given file; for instance, there was no way to distinguish between a neutron-gamma coupled set and neutron-induced gamma production.

4. There was no provision for coupled vector cross sections. Even when the matrix data are coupled, the vector data would not be.

5. There was a number of less significant points, including our belief that material composition data do not belong in the file.

Consequently, we chose to specify a new file MATXS to solve these problems and to incorporate other features which we felt were desirable. In addition, the new file was designed with the flexibility to incorporate additional data types, such as self-shielding factors, delayed neutron data, and delayed photon spectra.

Tentative agreement has been reached between LASL and ORNL to cooperate on the further development of the MATXS file. We have written a code which will translate an existing ISOTXS file into MATXS format and a general printing routine for MATXS. ORNL is developing a code to convert ANISN format to MATXS. These codes will be exchanged, and additional development is also under way.

H. MINX vs MC^2 (R. B. Kidman)

The Processing Code Subcommittee of the Code Evaluation Working Group has specified a simple reactor system that can be used to test and compare various code systems. The problem is a zero-leakage, infinite, homogeneous, ZPR-6-7, with the inner-core composition at 300°. All code systems are to begin with ENDF/B-IV data.[34] In an earlier comparison, the MINX/1DX system[33,35] used at LASL gave an eigenvalue of 1.2140, whereas the MC^2 system[36] used at Argonne National Laboratory (ANL) generated a multiplication of 1.2092. A detailed investigation was initiated this quarter in an effort to explain this difference.

Collapsed 28-group cross sections from MC^2 were put into the 1DX format and compared on a group-to-group basis with collapsed 28-group cross sections

from the MINX/1DX system. An example of the comparison is shown in Table III for the ^{239}Pu group cross sections. The results in Table III are percentage differences computed in the following manner.

$$\% \text{ Difference} = \frac{(MC^2 \text{ X-sec}) - (\text{MINX/1DX X-sec})}{(\text{MINX/1DX X-sec})} \times 100 \quad .$$

In Table III, 100.00 means that the MINX/1DX X-sec = 0, while the MC^2 X-sec $\neq$ 0; -100.00 means that the MINX/1DX X-sec $\neq$ 0, while the MC^2 X-sec = 0. Similar results are available for every isotope in the composition and for the macroscopic cross sections of the mix.

Exact perturbation can be used to determine what effect each cross section difference has on the K_∞ difference. In addition to the cross sections, adjoint flux and K_∞ from the MINX/1DX system, this method requires the regular flux and K_∞ one obtains by running the 1DX-formatted MC^2 cross sections through 1DX. This was first done using the fission source that LASL used in the MINX/1DX testing. The resulting eigenvalue of 1.2118 was worrisome since it did not duplicate the original MC^2 value of 1.2092. However, when the MC^2 fission source was used with the MC^2 cross sections in a 1DX run, the original MC^2 eigenvalue was duplicated. Thus, instead of the original $K_{\infty B}$ difference of 0.0048, we are now trying to explain a difference of only 0.0022.

Following through with exact perturbation theory, we can determine the components of ΔK_∞ as shown in Table IV. An example of the particular effects of cross-section differences on the final ΔK_∞ is shown in Table V for ^{239}Pu. The numbers in this table actually represent the following calculation

$$\% \text{ Effect} = \frac{\delta K_\infty \text{ caused by X-sec difference}}{\text{Total } \Delta K_\infty} \times 100 \quad .$$

One should not be alarmed at the number and size of compensating effects in Table V for this is a normal consequence of analyzing smaller and smaller integral parameter differences. As before, similar results are available for every isotope in the composition and for the macroscopic cross sections of the mix.

Thus far we have explained ~50% of the MINX/1DX vs MC^2 difference. We have also laid the groundwork for further investigation by clearly and conveniently presenting cross-section differences and their effect on K_∞.

TABLE III

PERCENTAGE DIFFERENCES BETWEEN MINX/1DX AND MC^2 CROSS SECTIONS FOR ^{239}Pu

I	SIGF	SIGA	NUSIGF	SIGTR	GXG	G=1XG	G=2XG	G=3XG	G=4XG	G=5XG	G=6XG	G=7XG	G=8XG	G=9XG	G=10XG
1	-1.22	-.76	-2.69	1.27	4.34	0.00	0.00	0.00	0.00	0.00	0.00	0.00	0.00	0.00	0.00
2	.22	.03	-.01	-.13	.17	-14.98	0.00	0.00	0.00	0.00	0.00	0.00	0.00	0.00	0.00
3	.52	.54	.23	.63	1.17	-6.98	9.36	0.00	0.00	0.00	0.00	0.00	0.00	0.00	0.00
4	-.31	-.29	-.41	.13	-.18	5.92	-.04	8.80	0.00	0.00	0.00	0.00	0.00	0.00	0.00
5	-.00	-.32	-.53	.49	1.39	4.22	-2.72	.26	7.08	0.00	0.00	0.00	0.00	0.00	0.00
6	-.38	-.18	-.51	.86	.74	-2.04	.18	-1.46	.15	4.54	0.00	0.00	0.00	0.00	0.00
7	.33	-.33	-.24	-.43	-.95	7.56	8.30	-2.36	-.64	.21	1.94	0.00	0.00	0.00	0.00
8	.32	.31	-.38	-.11	-1.26	5.44	-2.70	-5.24	-1.67	-.13	.03	-1.86	0.00	0.00	0.00
9	.31	.21	-.10	-.18	-.14	22.22	1.31	4.92	-2.02	-1.21	.18	-40.95	-38.77	0.00	0.00
10	-.34	.24	-.16	.15	-.31	-3.14	6.99	-.24	6.73	4.47	-40.97	-39.37	100.00	100.00	0.00
11	-.34	-.39	-.16	-.39	-.26	8.26	2.13	-1.92	-2.23	-38.63	-36.84	100.00	100.00	100.00	100.00
12	.26	.38	-.26	.20	-1.20	6.57	-5.24	-2.81	-5.92	-43.29	100.00	100.00	100.00	100.00	100.00
13	-.54	-1.25	-.78	1.21	1.89	39.39	0.00	2.56	35.27	-23.90	100.00	100.00	100.00	100.00	100.00
14	-.60	-1.22	-.76	.92	1.30	-2.22	0.00	15.15	10.34	-28.22	100.00	100.00	100.00	100.00	100.00
15	-.93	-.75	-.96	.33	.23	1.72	-14.85	0.00	8.70	-50.47	100.00	100.00	100.00	100.00	100.00
16	-1.96	-1.31	-1.98	.20	.89	2.29	-6.45	0.00	0.00	-29.72	100.00	100.00	100.00	100.00	100.00
17	-5.39	-3.24	-5.20	-2.26	-2.41	-15.13	0.00	8.82	0.00	0.00	100.00	100.00	100.00	100.00	100.00
18	-.82	-.89	-.94	1.85	3.51	14.38	0.00	-100.00	-7.71	0.00	0.00	100.00	100.00	100.00	100.00
19	-2.93	-2.46	-3.05	2.96	7.82	4.50	0.00	0.00	15.23	-39.63	0.00	0.00	100.00	100.00	100.00
20	-1.03	-1.16	-1.15	7.62	19.27	.88	0.00	0.00	0.00	-36.94	0.00	0.00	0.00	100.00	100.00
21	3.67	2.29	3.54	7.76	14.95	-12.78	0.00	0.00	0.00	0.00	100.00	0.00	0.00	0.00	100.00
22	5.34	6.33	5.21	17.93	51.34	-22.46	0.00	0.00	0.00	0.00	0.00	100.00	0.00	0.00	0.00
23	-19.24	-19.75	-19.34	6.32	120.92	10.78	0.00	0.00	0.00	0.00	0.00	0.00	100.00	0.00	0.00
24	3.94	1.62	3.72	26.46	9766.47	-7.17	0.00	0.00	0.00	0.00	0.00	0.00	0.00	100.00	0.00
25	148.94	73.26	148.54	124.69	-285.84	-9.60	0.00	0.00	0.00	0.00	0.00	0.00	0.00	0.00	100.00
26	-29.33	-28.61	-29.41	5.93	83.12	15.62	0.00	0.00	0.00	0.00	0.00	0.00	0.00	0.00	0.00
27	9.72	11.30	8.58	64.55	-165.20	53.90	0.00	0.00	0.00	0.00	0.00	0.00	0.00	0.00	0.00
28	6314.58	7596.27	6389.45	4551.96	-12.37	524.32	0.00	0.00	0.00	0.00	0.00	0.00	0.00	0.00	0.00

TABLE IV

COMPONENTS OF MINX/1DX vs MC^2 ZPR-6-7 K_∞ DIFFERENCE

Component	δK_∞	% of ΔK_∞
Absorption	+ 0.002449	+ 107.84
Fission	- 0.009201	- 405.15
Downscatter	+ 0.004481	+ 197.31
Total (ΔK)	- 0.002271	- 100.00

TABLE V

PERCENTAGE EFFECTS OF MINX/1DX vs MC^{2} ^{239}Pu CROSS-SECTION DIFFERENCES ON THE FINAL ΔK_{∞}

I	SIGF	SIGA	NUSIGF	SIGTR	GXG	G=1XG	G=2XG	G=3XG	G=4XG	G=5XG	G=6XG	G=7XG	G=8XG	G=9XG	G=10XG
1	0.000	-.481	4.872	0.000	0.000	0.000	0.000	0.000	0.000	0.000	0.000	0.000	0.000	0.000	0.000
2	0.000	.048	-.064	0.000	0.000	.033	0.000	0.000	0.000	0.000	0.000	0.000	0.000	0.000	0.000
3	0.000	2.718	-2.840	0.000	0.000	-.005	-.017	0.000	0.000	0.000	0.000	0.000	0.000	0.000	0.000
4	0.000	-2.058	7.240	0.000	0.000	-.393	.001	-.067	0.000	0.000	0.000	0.000	0.000	0.000	0.000
5	0.000	-2.410	10.585	0.000	0.000	-.747	.393	-.004	-.117	0.000	0.000	0.000	0.000	0.000	0.000
6	0.000	-2.002	17.343	0.000	0.000	.129	-.020	.251	-.210	-.076	0.000	0.000	0.000	0.000	0.000
7	0.000	-.317	1.255	0.000	0.000	-1.393	-.698	.230	.299	-.012	-.025	0.000	0.000	0.000	0.000
8	0.000	.145	3.047	0.000	0.000	-.513	.374	.240	.151	.013	-.001	.015	0.000	0.000	0.000
9	0.000	.278	4.122	0.000	0.000	-2.255	-.061	-.424	.270	.067	-.029	1.273	.255	0.000	0.000
10	0.000	.634	6.240	0.000	0.000	.388	-.294	.208	-.302	-.084	1.998	1.739	-.874	-.188	0.000
11	0.000	-1.100	5.239	0.000	0.000	-.721	-.090	.057	.052	1.749	.610	-1.362	-1.198	-.366	-.132
12	0.000	2.861	1.522	0.000	0.000	-.379	.069	.022	.117	.860	-1.495	-.460	-.581	-.489	.254
13	0.000	-11.731	22.445	0.000	0.000	-1.300	0.000	-.023	-.063	.266	-.645	-.573	-.182	-.230	-.301
14	0.000	-9.910	17.662	0.000	0.000	.023	0.000	-.002	-.239	.112	-.185	-.174	-.267	-.063	-.139
15	0.000	-5.247	14.562	0.000	0.000	.016	-.017	0.000	-.003	.032	-.074	-.088	-.061	-.082	-.036
16	0.000	-7.822	22.757	0.000	0.000	.025	-.051	0.000	0.000	.023	-.015	-.020	-.031	-.024	-.043
17	0.000	-10.294	27.439	0.000	0.000	-.060	0.000	.051	0.000	0.000	.001	-.203	-.239	-.018	-.019
18	0.000	-9.526	18.752	0.000	0.000	.095	0.000	-.001	-.235	0.000	0.000	.002	-.020	-.023	-.025
19	0.000	-25.685	59.835	0.000	0.000	.049	0.000	0.000	.022	-.003	0.000	0.000	.002	.004	-.021
20	0.000	-12.744	17.151	0.000	0.000	.016	0.000	0.000	0.000	-.057	0.000	0.000	0.000	.021	.004
21	0.000	10.739	-26.163	0.000	0.000	-.024	0.000	0.000	0.000	0.000	.036	0.000	0.000	0.000	.021
22	0.000	24.522	-28.457	0.000	0.000	-.102	0.000	0.000	0.000	0.000	0.000	.018	0.000	0.000	0.000
23	0.000	-23.689	42.634	0.000	0.000	-.011	0.000	0.000	0.000	0.000	0.000	0.000	.035	0.000	0.000
24	0.000	1.380	-4.852	0.000	0.000	-.014	0.000	0.000	0.000	0.000	0.000	0.000	0.000	.023	0.000
25	0.000	6.732	-19.346	0.000	0.000	.005	0.000	0.000	0.000	0.000	0.000	0.000	0.000	0.000	.021
26	0.000	-.058	.161	0.000	0.000	-.000	0.000	0.000	0.000	0.000	0.000	0.000	0.000	0.000	0.000
27	0.000	.036	-.041	0.000	0.000	.000	0.000	0.000	0.000	0.000	0.000	0.000	0.000	0.000	0.000
28	0.000	.002	-.003	0.000	0.000	-.000	0.000	0.000	0.000	0.000	0.000	0.000	0.000	0.000	0.000

I. Leakage Corrections to Self-Shielded Cross Sections (R. B. Kidman)

Last quarter, several methods were introduced for adding zone-dependent leakage corrections to the background cross section σs_0. The correction which yielded the largest changes is given by

$$\sigma^g_{0,m,eff} = \sigma^g_{0,m} + \frac{2B^g_z}{\pi N_{m,z}} \tag{7}$$

where

$$B^g_z = \sqrt{\left| \frac{L^g_z}{D^g_z \phi^g_z V_z} \right|}$$

L^g_z = leakage rate from zone z for group g

ϕ^g_z = average flux for group g in zone z

V_z = volume of zone z

D^g_z = diffusion coefficient for group g in zone z

$N_{m,z}$ = atom density for material m in zone z. (8)

This change increased the very low ZPR-III-54 eigenvalue by only ~1.5%. This fact, plus a serendipitous interpretation of a fortuitous error made during the implementation of Eq. (7), led M. Becker of Rensselaer Polytechnic Institute (RPI) to re-examine the traditional formula for the diffusion coefficient. If D is defined as the current-to-flux ratio

$$D = -\frac{J}{iB\phi} \quad , \tag{9}$$

one can use a flux given by the B_0 approximation and a current given by the B_1 approximation to obtain

$$D_z^g = \frac{1 - \frac{\Sigma_z^g}{B_z^g} \tan^{-1}\left(\frac{B_z^g}{\Sigma_z^g}\right)}{B_z^g \tan^{-1}\left(\frac{B_z^g}{\Sigma_z^g}\right)\left[1 + \frac{3\Sigma_z^g \Sigma_{s,z}^g}{B_z^g} \frac{\frac{\Sigma_z^g}{B_z^g} \tan^{-1}\left(\frac{B_z^g}{\Sigma_z^g}\right) - 1}{B_z^g}\right]} , \quad (10)$$

where Σ_z^g is the microscopic total cross section for group g in zone z, and $\Sigma_{s,z}^g$ is the microscopic scattering cross section. Equation (10) reduces to the conventional $1/3\Sigma_{tr}$ for small B/Σ.

After Eq. (10) was also incorporated into 1DX,[35] we obtained 1.014 for the ZPR-III-54 eigenvalue as compared to 0.9532 with the unmodified 1DX (including in both cases a net correction of + 0.021 for heterogeneity, dimensionality, and transport effects[37]). The new eigenvalue is encouraging because ZPR-III-54 now no longer stands out as a singularly bad critical assembly.

We have also analyzed ZPR-6-7 which is a much larger and therefore less leaky system. The change in multiplication for ZPR-6-7 (0.9708 → 0.9747, uncorrected eigenvalues) is about 15 times smaller than that for ZPR-III-54 and in a direction to also improve agreement with experiment. Thus, our leakage corrections appear to produce large effects when and where they are needed, and to generate small effects when leakage is relatively small.

In summary, this work has successfully identified and incorporated zone leakage corrections into the Shielding Factor Method and has demonstrated that their application can remove the long-standing low-eigenvalue problem of ZPR-III-54 with no significant penalties in computer time and with no additional problem requirements.

J. Spectral Corrections to Elastic Removal Cross Sections (R. B. Kidman)

Since more accurate multigroup elastic removal cross sections[38] have become available, it is appropriate to consider a new method for adjusting these cross sections to problem dependent spectra.

This is now done in 1DX[2] via an iterative procedure between flux ϕ and elastic removal cross section, σ_r. At each iteration, the authors use a linear interpolation between $\bar{\xi}^{i}\bar{\sigma}^{i}\phi(u^{i})$ and $\bar{\xi}^{i+1}\bar{\sigma}_e^{i+1}\phi(u^{i+1})$ to determine the value at $u^{i}-.66\bar{\xi}^{i}$ and then assume

$$\bar{\sigma}_r^{i} = \bar{\xi}\bar{\sigma}_e\phi\Big|_{u^{i}-.66\bar{\xi}^{i}}\Big/\phi^{i} \quad , \tag{11}$$

where i is the group index, $\bar{\xi}$ is the average logrithmic energy decrement, $\bar{\sigma}_e$ is the effective elastic scattering cross section, u is the lethargy, and $\phi^{i} = \int^{i}\phi(u)du$.

As Eq. (11) reveals, the locations of elastic scattering resonances do not directly influence the elastic removal cross section. This scheme was probably adopted because up to now the elastic removal cross sections provided to 1DX were also generated without directly accounting for scattering resonance locations.

The elastic removal cross sections provided by LIB-IV were calculated according to the following algorithm.

$$\sigma_{ro}^{i} = \int^{\alpha} dE\phi_0(E)\sigma_e(E)P(E\rightarrow E'<E_{i+1})\Big/\int^{i} dE\phi_0(E) \quad , \tag{12}$$

where $\int^{\alpha}$ is an integration over that part of group i which can possibly elastically scatter a neutron out of the group, $\int^{i}$ is an integration over group i, E is the energy, $\phi_0(E)$ is the arbitrary intragroup flux weighting spectrum, $\sigma_e(E)$ is the elastic scattering cross section, and $P(E\rightarrow E'<E_{i+1})$ is the fractional probability that an elastically scattered neutron of initial energy E will be scattered out of group i. Equation (12) explicitly accounts for scattering resonance locations in the computation of elastic removal cross sections.

The new method makes simplifying assumptions about the intragroup shape of ϕ_0, ϕ, σ_e, and P in order to compute two new values of the elastic removal cross section

$$\sigma_{r1}^{i} = \int^{\alpha} du\ \phi_0'(u)\ \sigma_e'(u)\ P'(u) \Big/ \int^{i} du\ \phi_0'(u) \quad , \tag{13}$$

$$\sigma_{r2}^{i} = \int^{\alpha} du\ \phi'(u)\ \sigma_e'(u)\ P'(u) \Big/ \int^{i} du\ \phi'(u) \quad , \tag{14}$$

where the primes refer to the assumed simplified shapes. The $\phi_0'(u)$, $\phi'(u)$, and $\sigma_e^i(u)$ shapes are derived from 3-point Lagrange interpolation schemes, while $P'(u)$ is simply given a linear shape.

The relative values of σ_{r1}^{i} and σ_{r2}^{i} are a measure of how the gross intragroup behavior of ϕ_0 and ϕ can affect the removal cross section. Thus, at each iteration in the new method a new effective elastic removal cross section is computed by

$$\bar{\sigma}_r^i = F_e^i\ \sigma_{r0}^i\ \sigma_{r2}^i \Big/ \sigma_{r1}^i \quad , \tag{15}$$

where F_e^i is the elastic self-shielding factor. First order cross-section changes required by an averaging with the new flux ϕ are thus introduced without losing the dependence on resonance location since all iterations are directly related to the original cross section.

Results from the new procedure and 1DX are compared in Table VI which shows the final ZPR-III-54 ^{238}U elastic removal cross sections in terms of the initial cross sections. The striking feature of these results is the much larger changes developed by 1DX than by the new scheme. Similar results exist for all isotopes in the composition. The new eigenvalue is ~0.9% less than the 1DX eigenvalue.

Since the LIB-IV elastic removal cross sections are very realistic, the new method for introducing spectral changes appears to give much more reasonable results than the old 1DX method. Future work will consist of introducing better self-shielding effects for the transfer cross sections, introducing spectral corrections to all cross sections and, of course, establishing the effect of all of these modifications on more than one critical assembly.

TABLE VI

A COMPARISON OF TWO SPECTRAL COMPARISON SCHEMES ON ZPR-III-54 ^{238}U ELASTIC REMOVAL X-SEC

Group	LIB-IV Initial $\bar{\sigma}_r$ (barns)	1DX Final $\bar{\sigma}_r$ ÷ Initial $\bar{\sigma}_r$	New Method Final $\bar{\sigma}_r$ ÷ Initial $\bar{\sigma}_r$
1	.0322	1.0000	.7553
2	.0284	1.7225	1.0402
3	.0277	1.3767	1.1308
4	.0298	1.1838	1.1782
5	.0308	1.2489	1.1968
6	.0422	1.3071	1.1506
7	.0784	.9860	1.0313
8	.1848	1.0027	1.0204
9	.2167	.9759	.9934
10	.2479	.9690	.9679
11	.2768	.9785	.9547
12	.3048	.9836	.9911
13	.3375	.9649	.9772
14	.3647	.9800	.9886
15	.3870	.9742	.9766
16	.4086	.9708	.9738
17	.4152	.9521	.9527
18	.4248	.9752	1.0047
19	.4367	1.0174	.9913
20	.4435	.9570	.9448
21	.4533	.9706	.9624
22	.4618	.9552	.9724
23	.4704	.9467	.9521
24	.4846	.9717	.9584
25	.4938	.9645	.9710
26	.5031	1.0088	.9773
27	.3662	1.3920	.9687
28	.5210	.9568	.9590
29	.3551	1.4957	.9517
30	.9004	.5434	.9494
31	1.1823	.3741	.9412
32	.3099	1.4371	.9361
33	.2253	1.8655	.9353
34	.2109	1.8681	.9184
35	.2541	1.4144	.9180
36	.4264	.8581	.9142
37	.2859	1.5043	.8948
38	.0399	5.8707	.7525
39	3.1446	.0595	.7209
40	.0355	4.2387	.6786
41	1.5052	.1425	.7551
42	.0264	5.1150	.7748
43	.0300	4.6318	.6656
44	.1772	.6868	.7694
45	.0510	3.3696	.9271
46	.1408	.9934	1.0242
47	.1461	.7461	.8451
48	.1486	.5938	.5908
49	.1499	.9550	.9809
50	.0000	0.0000	0.0000

K. Effects of Weighting Spectra on Group Collapse (R. B. Kidman)

The purpose of this study is to compare the effects of group collapsing with an actual spectrum vs collapsing with an arbitrary spectrum. We have performed this comparison using the Processing Codes Subcommittee's infinite homogeneous ZPR-6-7 specification. The procedure is outlined in Fig. 10.

If one begins with the 50-group CCCC[39] format library LIB-IV,[38] uses CINX[40] to convert a 50-group 1DX[35] format library, and performs a K_∞ and 28-group crunch calculation with 1DX, a value of K_∞ = 1.2140487 is obtained. On the other hand, if one begins with LIB-IV, uses CINX to crunch and convert to a 28-group 1DX format library, and then performs a K_∞ calculation with 1DX, he will obtain K'_∞ = 1.2191568. Thus, for this problem, we see that collapsing with an arbitrary flux increases K_∞ by 0.0051081, or 0.42%.

Looking further and in more detail, Tables VII and VIII show, respectively, the ^{239}Pu resonance-shielded cross sections resulting from collapsing with the actual spectrum and from collapsing with the arbitrary spectrum. (In the interest of presenting compact tables, the uninteresting G-9XG and G-10XG terms were dropped.) Table IX is a more convenient and comprehensible percentage comparison between Tables VII and VIII

$$\text{Table IX} = \frac{\text{Table VIII} - \text{Table VII}}{\text{Table VII}} \times 100 \quad .$$

To determine how each of these differences affects K_∞, we have invoked exact perturbation theory (which combines the cross-section differences, flux, adjoint flux, K_∞, K'_∞, and material densities). Table X shows what percentage of the final ΔK_∞ (= 0.0051081) is caused by each cross-section difference.

What we find is an enormous number of differences that need to be explained. The ~40% differences in the transfer cross sections of Table IX are a result of *truncation* effects caused by limiting the number of downscattering terms to 10 in both CINX runs. All of the other differences and effects are real and are caused by the different weighting spectra used. Notice that groups 2-6 and 22-26 display the fewest changes because these groups also exist in the 50-group structure. (Group 27 is composed of 3 fine groups, group 28 is composed of 5 fine groups, and each of the unmentioned rest is composed of 2 fine groups.) Also note that there are a considerable number of compensating differences. Finally, one should note that the largest cross-section changes do not necessarily lead to the largest effects on K_∞.

TABLE VII

EFFECTIVE ^{239}Pu CROSS SECTIONS FROM 1DX COLLAPSE

I	SIGF	SIGA	NUSIGF	SIGTR	GXG	G-1XG	G-2XG	G-3XG	G-4XG	G-5XG	G-6XG	G-7XG	G-8XG
1	2.142E+00	2.009E+00	8.599E+00	3.564E+00	6.04AE-01	0.	0.	0.	0.	0.	0.	0.	0.
2	1.735E+00	1.736E+00	6.147E+00	4.282E+00	8.699E-01	6.465E-02	0.	0.	0.	0.	0.	0.	0.
3	1.882E+00	1.884E+00	6.171E+00	4.732E+00	1.300E+00	1.182E-01	5.518E-02	0.	0.	0.	0.	0.	0.
4	1.923E+00	1.934E+00	6.296E+00	4.972E+00	1.822E+00	3.474E-01	2.700E-01	1.446E-01	0.	0.	0.	0.	0.
5	1.749E+00	1.773E+00	5.294E+00	5.167E+00	2.459E+00	5.322E-01	3.350E-01	4.243E-01	2.165E-01	0.	0.	0.	0.
6	1.632E+00	1.705E+00	4.830E+00	5.868E+00	3.537E+00	5.387E-01	2.682E-01	3.576E-01	3.863E-01	2.018E-01	0.	0.	0.
7	1.554E+00	1.699E+00	4.559E+00	6.959E+00	4.826E+00	3.226E-01	2.349E-01	1.928E-01	2.546E-01	2.484E-01	1.363E-01	0.	0.
8	1.492E+00	1.682E+00	4.337E+00	7.922E+00	5.899E+00	2.844E-01	1.738E-01	8.728E-02	1.188E-01	1.435E-01	1.290E-01	7.525E-02	0.
9	1.533E+00	1.751E+00	4.457E+00	9.379E+00	7.320E+00	2.528E-01	8.887E-02	7.387E-02	4.643E-02	6.006E-02	6.622E-02	9.915E-02	5.581E-02
10	1.589E+00	1.886E+00	4.586E+00	1.079E+01	8.664E+00	2.455E-01	4.648E-02	3.188E-02	2.895E-02	2.171E-02	4.502E-02	4.691E-02	0.
11	1.643E+00	2.017E+00	4.619E+00	1.192E+01	9.659E+00	2.887E-01	4.404E-02	2.243E-02	1.673E-02	2.371E-02	1.449E-02	0.	0.
12	1.629E+00	2.109E+00	4.602E+00	1.273E+01	1.051E+01	2.456E-01	1.976E-02	6.150E-03	1.236E-02	1.233E-02	0.	0.	0.
13	1.686E+00	2.413E+00	4.849E+00	1.329E+01	1.047E+01	3.107E-01	0.	1.130E-02	1.252E-03	6.475E-03	0.	0.	0.
14	1.816E+00	2.823E+00	5.222E+00	1.402E+01	1.093E+01	2.789E-01	0.	4.263E-04	4.366E-03	2.744E-03	0.	0.	0.
15	2.092E+00	3.533E+00	6.014E+00	1.527E+01	1.155E+01	1.846E-01	3.905E-02	0.	1.315E-03	8.371E-04	0.	0.	0.
16	2.448E+00	4.515E+00	7.020E+00	1.671E+01	1.210E+01	1.793E-01	5.088E-02	0.	0.	8.720E-04	0.	0.	0.
17	3.179E+00	6.493E+00	9.134E+00	1.967E+01	1.260E+01	9.832E-02	0.	2.356E-02	0.	0.	0.	0.	0.
18	4.239E+00	7.385E+00	1.161E+01	1.948E+01	1.190E+01	4.932E-01	0.	4.687E-05	1.216E-02	0.	0.	0.	0.
19	5.992E+00	1.047E+01	1.722E+01	2.240E+01	1.176E+01	1.885E-01	0.	0.	5.355E-03	1.500E-04	0.	0.	0.
20	7.945E+00	1.441E+01	2.283E+01	2.587E+01	1.130E+01	1.697E-01	0.	0.	0.	3.068E-03	0.	0.	0.
21	8.793E+00	1.598E+01	2.526E+01	2.648E+01	1.053E+01	1.583E-01	0.	0.	0.	0.	0.	0.	0.
22	1.450E+01	2.697E+01	4.165E+01	3.653E+01	9.398E+00	1.722E-01	0.	0.	0.	0.	0.	0.	0.
23	1.597E+01	3.049E+01	4.589E+01	3.745E+01	6.813E+00	1.619E-01	0.	0.	0.	0.	0.	0.	0.
24	3.731E+01	5.326E+01	1.072E+02	5.338E+01	-1.209E-02	1.463E-01	0.	0.	0.	0.	0.	0.	0.
25	3.282E+01	5.973E+01	8.621E+01	5.230E+01	-7.560E+00	1.370E-01	0.	0.	0.	0.	0.	0.	0.
26	8.214E+00	1.630E+01	2.360E+01	2.200E+01	5.568E+00	1.202E-01	0.	0.	0.	0.	0.	0.	0.
27	5.899E+01	8.221E+01	1.465E+02	6.317E+01	-1.905E+01	8.748E-02	0.	0.	0.	0.	0.	0.	0.
28	1.158E+01	1.314E+01	3.326E+01	2.190E+01	8.764E+00	2.404E-03	0.	0.	0.	0.	0.	0.	0.

TABLE VIII

EFFECTIVE ^{239}Pu CROSS SECTIONS FROM CIXN COLLAPSE

I	SIGF	SIGA	NUSIGF	SIGTR	GXG	G-1XG	G-2XG	G-3XG	G-4XG	G-5XG	G-6XG	G-7XG	G-8XG
1	2.141E+00	2.809E+00	8.581E+00	3.568E+00	6.193E-01	0.	0.	0.	0.	0.	0.	0.	0.
2	1.735E+00	1.736E+00	6.147E+00	4.262E+00	8.695E-01	5.256E-02	0.	0.	0.	0.	0.	0.	0.
3	1.888E+00	1.884E+00	6.171E+00	4.732E+00	1.304E+00	1.187E-01	5.521E-02	0.	0.	0.	0.	0.	0.
4	1.923E+00	1.934E+00	6.886E+00	4.972E+00	1.821E+00	3.472E-01	2.704E-01	1.449E-01	0.	0.	0.	0.	0.
5	1.749E+00	1.773E+00	5.294E+00	5.167E+00	2.453E+00	5.331E-01	3.354E-01	4.243E-01	2.169E-01	0.	0.	0.	0.
6	1.632E+00	1.708E+00	4.83PE+00	5.868E+00	3.525E+00	5.359E-01	2.682E-01	3.576E-01	3.863E-01	2.022E-01	0.	0.	0.
7	1.557E+00	1.69AE+00	4.561E+00	6.883E+00	4.763E+00	3.338E-01	2.349E-01	1.928E-01	2.546E-01	2.484E-01	1.366E-01	0.	0.
8	1.492E+00	1.682E+00	4.337E+00	7.943E+00	5.922E+00	2.717E-01	1.738E-01	8.728E-02	1.188E-01	1.405E-01	1.290E-01	7.332E-02	0.
9	1.533E+00	1.751E+00	4.437E+00	9.368E+00	7.314E+00	2.509E-01	8.681E-02	7.387E-02	4.643E-02	6.006E-02	6.622E-02	5.868E-02	3.41PE-02
10	1.569E+00	1.885E+00	4.585E+00	1.078E+01	8.657E+00	2.490E-01	4.630E-02	3.347E-02	2.895E-02	2.171E-02	2.602E-02	2.834E-02	2.459E-02
11	1.609E+00	2.017E+00	4.620E+00	1.192E+01	9.653E+00	2.814E-01	4.407E-02	2.248E-02	1.678E-02	1.355E-02	8.892E-03	1.111E-02	1.143E-02
12	1.621E+00	2.113E+00	4.665E+00	1.275E+01	1.053E+01	2.473E-01	1.984E-02	6.155E-03	1.244E-02	7.338E-03	6.263E-03	3.498E-03	4.390E-03
13	1.6AAE+00	2.424E+00	4.856E+00	1.325E+01	1.051E+01	3.107E-01	0.	1.129E-02	1.251E-03	4.542E-03	3.362E-03	2.337E-03	1.334E-03
14	1.821E+00	2.834E+00	5.238E+00	1.405E+01	1.092E+01	2.715E-01	0.	4.328E-04	4.356E-03	1.713E-03	1.107E-03	1.027E-03	1.027E-03
15	2.092E+00	3.537E+00	6.014E+00	1.526E+01	1.156E+01	2.032E-01	4.451E-02	0.	1.335E-03	5.516E-04	6.457E-04	5.217E-04	4.681E-04
16	2.495E+00	4.597E+00	7.178E+00	1.686E+01	1.210E+01	1.473E-01	4.709E-02	0.	0.	5.385E-04	1.817E-04	2.409E-04	2.131E-04
17	3.3?3E+00	6.433E+00	9.491E+00	1.982E+01	1.296E+01	1.564E-01	0.	2.639E-02	0.	0.	2.164E-04	6.214E-05	8.959E-05
18	4.?3?E+00	7.382E+00	1.158E+01	1.949E+01	1.193E+01	4.316E-01	0.	4.581E-05	1.358E-02	0.	0.	8.189E-05	2.317E-05
19	5.953E+00	1.042E+01	1.710E+01	2.234E+01	1.174E+01	1.781E-01	0.	0.	5.234E-03	1.675E-04	0.	0.	3.049E-05
20	8.673E+00	1.521E+01	2.492E+01	2.668E+01	1.129E+01	1.729E-01	0.	0.	0.	1.886E-03	0.	0.	0.
21	9.216E+00	1.713E+01	2.648E+01	2.831E+01	1.181E+01	1.747E-01	0.	0.	0.	0.	6.999E-04	0.	0.
22	1.45?E+01	2.697E+01	4.165E+01	3.653E+01	9.398E+00	1.776E-01	0.	0.	0.	0.	0.	2.607E-04	0.
23	1.597E+01	3.049E+01	4.589E+01	3.745E+01	6.813E+00	1.619E-01	0.	0.	0.	0.	0.	0.	9.688E-05
24	3.731E+01	5.326E+01	1.072E+02	5.338E+01	-1.223E-02	1.403E-01	0.	0.	0.	0.	0.	0.	0.
25	3.?20E+01	5.973E+01	8.621E+01	5.230E+01	-7.557E+00	1.371E-01	0.	0.	0.	0.	0.	0.	0.
26	8.214E+00	1.634E+01	2.36?E+01	2.200E+01	5.541E+00	1.252E-01	0.	0.	0.	0.	0.	0.	0.
27	4.226E+01	6.754E+01	1.214E+02	5.242E+01	-1.517E+01	1.144E-01	0.	0.	0.	0.	0.	0.	0.
28	3.052E+02	4.437E+02	8.770E+02	2.284E+02	-2.153E+02	4.453E-02	0.	0.	0.	0.	0.	0.	0.

TABLE IX

PERCENTAGE DIFFERENCES BETWEEN 1DX AND CINX COLLAPSED ^{239}Pu CROSS SECTIONS

I	SIGF	SIGA	NUSIGF	SIGTR	GXG	G-1XG	G-2XG	G-3XG	G-4XG	G-5XG	G-6XG	G-7XG	G-8XG	G-9XG	G-10XG
1	-.00	-.02	-.11	.11	2.41	0.00	0.00	0.00	0.00	0.00	0.00	0.00	0.00	0.00	0.00
2	-.00	-.00	-.00	0.00	-.05	-18.69	0.00	0.00	0.00	0.00	0.00	0.00	0.00	0.00	0.00
3	-.00	-.00	-.00	-.00	.01	.39	.21	0.00	0.00	0.00	0.00	0.00	0.00	0.00	0.00
4	-.00	-.00	-.00	0.00	-.05	-.05	0.00	.17	0.00	0.00	0.00	0.00	0.00	0.00	0.00
5	-.00	-.00	-.00	0.00	.12	.16	0.00	0.00	.18	0.00	0.00	0.00	0.00	0.00	0.00
6	-.00	-.00	-.00	-.00	-.32	-.53	0.00	0.00	0.00	.20	0.00	0.00	0.00	0.00	0.00
7	.20	-.02	.24	-1.09	-1.30	3.50	0.00	0.00	0.00	-.00	.22	0.00	0.00	0.00	0.00
8	-.00	-.00	-.00	.26	.39	-4.47	.00	0.00	.00	-.00	-.00	-2.57	0.00	0.00	0.00
9	-.00	-.00	-.00	-.12	-.20	-.77	-2.33	0.00	0.00	0.00	0.00	-40.82	-38.91	0.00	0.00
10	-.01	-.02	-.01	-.13	-.08	1.43	-.40	4.99	0.00	0.00	-40.42	-39.60	.02	.01	0.00
11	.02	.01	.02	-.00	-.02	-3.52	.06	.21	.27	-42.84	-38.61	.01	.01	.01	.01
12	.05	.18	.05	.16	.16	.68	.39	.07	.64	-40.47	.01	.00	.00	.00	.01
13	.15	.45	.15	.34	.35	.02	0.00	-.13	-.07	-29.85	.00	.00	.00	.00	.00
14	.23	.41	.23	.16	-.08	-2.65	0.00	1.53	-.22	-37.56	.00	.00	.00	.00	.00
15	.01	.12	.01	-.08	.13	10.05	13.97	0.00	1.53	-34.11	.00	.00	.00	.00	.00
16	2.02	1.02	2.02	.86	.03	-17.82	-5.98	0.00	0.00	-38.24	.00	.00	.00	.00	.00
17	3.91	-.93	3.91	.78	2.17	59.07	0.00	11.66	0.00	0.00	.00	.00	.00	.00	.00
18	-.22	-.03	-.22	.04	.18	-12.49	0.00	-2.27	11.66	0.00	0.00	.00	.00	.00	.00
19	-.66	-.43	-.66	-.27	-.15	-5.50	0.00	0.00	-2.27	11.66	0.00	0.00	.00	.00	.00
20	9.16	5.60	9.16	3.12	-.15	1.87	0.00	0.00	0.00	-38.50	0.00	0.00	0.00	.00	.00
21	4.81	7.15	4.81	6.91	6.60	10.37	0.00	0.00	0.00	0.00	.00	0.00	0.00	0.00	.00
22	-.00	-.00	-.00	-.00	-.00	3.15	0.00	0.00	0.00	0.00	0.00	.00	0.00	0.00	0.00
23	-.00	-.00	-.00	-.00	.00	.00	0.00	0.00	0.00	0.00	0.00	0.00	.00	0.00	0.00
24	-.00	-.00	-.00	.00	1.09	-.00	0.00	0.00	0.00	0.00	0.00	0.00	0.00	.00	0.00
25	-.00	-.00	-.00	-.00	-.04	.10	0.00	0.00	0.00	0.00	0.00	0.00	0.00	0.00	.00
26	-.00	-.00	-.00	-.00	-.48	-2.37	0.00	0.00	0.00	0.00	0.00	0.00	0.00	0.00	0.00
27	-17.14	-17.85	-17.14	-17.02	-20.38	30.78	0.00	0.00	0.00	0.00	0.00	0.00	0.00	0.00	0.00
28	2536.75	3276.51	2536.75	942.63	-2556.79	1752.56	0.00	0.00	0.00	0.00	0.00	0.00	0.00	0.00	0.00

TABLE X

PERCENTAGE OF ΔK CAUSED BY ^{239}Pu CROSS SECTION DIFFERENCES

I	SIGF	SIGA	NUSIGF	SIGTR	GXG	G-1XG	G-2XG	G-3XG	G-4XG	G-5XG	G-6XG	G-7XG	G-8XG	G-9XG	G-10XG
1	0.000	.005	-.009	0.000	0.000	0.000	0.000	0.000	0.000	0.000	0.000	0.000	0.000	0.000	0.000
2	0.000	.000	-.000	0.000	0.000	-.019	0.000	0.000	0.000	0.000	0.000	0.000	0.000	0.000	0.000
3	0.000	.000	-.000	0.000	0.000	-.000	.000	0.000	0.000	0.000	0.000	0.000	0.000	0.000	0.000
4	0.000	.000	-.000	0.000	0.000	-.001	0.000	.001	0.000	0.000	0.000	0.000	0.000	0.000	0.000
5	0.000	.000	-.000	0.000	0.000	.013	0.000	0.000	.001	0.000	0.000	0.000	0.000	0.000	0.000
6	0.000	.000	-.000	0.000	0.000	-.015	0.000	0.000	0.000	.002	0.000	0.000	0.000	0.000	0.000
7	0.000	.105	3.206	0.000	0.000	.225	0.000	0.000	0.000	-.000	.001	0.000	0.000	0.000	0.000
8	0.000	.008	-.067	0.000	0.000	-.184	.000	0.000	.000	-.000	-.000	-.000	0.000	0.000	0.000
9	0.000	.009	-.023	0.000	0.000	-.001	-.002	0.000	0.000	0.000	0.000	-.562	-.117	0.000	0.000
10	0.000	.159	-.124	0.000	0.000	.076	-.008	.073	0.000	0.000	-.872	-.737	.389	.086	0.000
11	0.000	-.028	.253	0.000	0.000	-.143	.001	.003	.003	-.865	-.296	.606	.504	.172	.001
12	0.000	-.767	.596	0.000	0.000	.017	.002	.000	.006	-.352	.598	.205	.258	.209	.114
13	0.000	-2.385	2.057	0.000	0.000	.000	0.000	-.001	-.000	-.158	.251	.234	.082	.163	.130
14	0.000	-1.588	2.169	0.000	0.000	-.013	0.000	.000	-.000	-.065	.093	.079	.105	.030	.003
15	0.000	-.434	.066	0.000	0.000	-.037	-.008	0.000	.000	-.010	.058	.042	.034	.034	.017
16	0.000	-4.143	8.825	0.000	0.000	.098	.019	0.000	0.000	-.002	.005	.012	.015	.012	.017
17	0.000	1.307	9.251	0.000	0.000	-.089	0.000	-.030	0.000	0.000	-.000	.001	.003	.005	.007
18	0.000	.172	-1.987	0.000	0.000	.037	0.000	.000	-.021	0.000	0.000	-.001	.000	.001	.002
19	0.000	2.095	-5.873	0.000	0.000	.028	0.000	0.000	.002	-.000	0.000	0.000	-.001	-.000	.000
20	0.000	-21.798	57.104	0.000	0.000	-.016	0.000	0.000	0.000	.000	0.000	0.000	0.000	-.001	-.000
21	0.000	-14.630	15.399	0.000	0.000	-.010	0.000	0.000	0.000	0.000	-.020	0.000	0.000	0.000	-.000
22	0.000	.000	-.000	0.000	0.000	-.006	0.000	0.000	0.000	0.000	0.000	-.010	0.000	0.000	0.000
23	0.000	.000	-.000	0.000	0.000	.000	0.000	0.000	0.000	0.000	0.000	0.000	-.000	0.000	0.000
24	0.000	.000	-.000	0.000	0.000	.000	0.000	0.000	0.000	0.000	0.000	0.000	0.000	-.000	0.000
25	0.000	.000	-.000	0.000	0.000	.000	0.000	0.000	0.000	0.000	0.000	0.000	0.000	0.000	-.001
26	0.000	.000	-.000	0.000	0.000	-.000	0.000	0.000	0.000	0.000	0.000	0.000	0.000	0.000	0.000
27	0.000	.177	-.253	0.000	0.000	-.000	0.000	0.000	0.000	0.000	0.000	0.000	0.000	0.000	0.000
28	0.000	-.095	.164	0.000	0.000	.000	0.000	0.000	0.000	0.000	0.000	0.000	0.000	0.000	0.000

Similar complete results for the other isotopes in the ZPR-6-7 composition and for the composition as a whole can also be provided upon request.

The value of this work is that for the first time the excruciating details of weighting function-caused differences are completely and conveniently presented to highlight the kinds of effects to be expected from using various weighting spectra. It will be interesting to repeat this work after 1DX has been modified for gross spectral changes on all cross sections. We would expect the differences to be much less than we see in the present work.

L. Improved Cross Sections for Thermal Reactor Analysis (R. E. MacFarlane and R. Boicourt)

With the support of the Electric Power Research Institute (EPRI), the NJOY nuclear data processing system is being extended to generate improved cross sections for use in the analysis of thermal power reactor systems. During this quarter, we have concentrated on developing improved data for EPRI-CELL.[41] This code is designed to produce self-homogenized few-group cross sections for typical power reactor cells. Thermal range calculations are based on THERMOS[42] and epithermal calculations are based on GAM-1[43] modified to use equivalence theory in the manner of the WIMS[44] system.

The thermal library for EPRI-CELL contains multigroup capture and fission cross sections, the group-to-group scattering matrices, and other quantities required for the thermal flux and power calculation. A new storage procedure has been implemented for the scattering matrices which cuts the storage required in half. Furthermore, a temperature interpolation capability has been added for both cross sections and matrices. Since all cross sections produced by NJOY have been accurately Doppler broadened, interpolating between temperatures on the library tape provides accurate cross sections with a smooth temperature dependence without requiring the use of resonance parameters. In addition, the size of the library can be further reduced since it is not necessary to provide scattering matrices at so many intermediate temperatures.

The fast library for EPRI-CELL contains cross sections for fission and capture; matrices for P_0 elastic, P_1 elastic, (n,2n), and inelastic scattering; self-shielding factors for fission and capture; and fission $\bar{\nu}$ and χ data. All these data are produced by the current version of NJOY; however, self-shielding factors are computed using the narrow-resonance approximation. In a thermal reactor, the strong broad and intermediate resonances in the 0.1-100 eV range

are very important. In order to treat these resonances more accurately, a simple infinite medium flux calculator has been added to NJOY. It is assumed that the heavy absorber is mixed with a light moderator so that all resonances are narrow with respect to moderator scattering. The weighting flux for group averaging is then obtained from

$$\phi(e) = \frac{F(E)}{\phi_0 + \phi_t(E)} \tag{16}$$

where F is the solution of

$$F(E) = \frac{1}{F} \int_E^{E/\alpha} \frac{\sigma_e(E')F(E')}{(1-\alpha)E'[\sigma_0 + \sigma_t(E')]} dE' \tag{17}$$

In these equations, σ_0 is the moderator cross section per absorber atom, σ_t is the total absorber cross sections, σ_e is the absorber scattering cross section, and $\alpha = (A-1)^2/(A+1)^2$. Equation (17) is solved by iteration, using the point-wise cross sections available within NJOY. Above some preselected energy, the solution is assumed to be $F = 1/E$ (i.e, the narrow resonance limit). This procedure gives self-shielding factors which incorporate broad resonance effects in a manner consistent with the equivalence principles used in EPRI-CELL.

III. HTGR CROSS SECTIONS AND DEPLETION CALCULATIONS FOR REACTOR SAFETY ANALYSIS (R. J. LaBauve, M. G. Stamatelatos, and T. R. England)

The LASL 9-group cross-section library for HTGR end-of-equilibrium cycle safety analysis has been expanded to include 21 nuclides. These are as follows.

	Nuclide	MAT NO.	ENDF/B-VERSION	Region
1.	B-10	1155	III	Core
2.	C-12	1165	III	"
3.	O-16	1134	III	"
4.	Si-28	1194	III	"
5.	Xe-135	1294	IV	"
6.	Sm-149	1027	I	"
7.	Th-232	1117	III	"
8.	Pa-233	1119	III	"
9.	Pa-233	1297	IV	"
10.	U-233	1260	IV	"
11.	U-234	1043	I	"
12.	U-235	1157	III	"
13.	U-236	1163	III	"
14.	U-238	1158	III	"
15.	Pu-238	1050	I	"
16.	Pu-239	1264	IV	"
17.	Pu-240	1265	IV	"
18.	Pu-241	1266	IV	"
19.	Pu-242	1161	III	"
20.	B-10	1155	III	reflector
21.	C-12	1165	III	reflector

Cross sections for every nuclide in the above list are available for 12 temperatures including 300, 500, 600, 800, 1000, 1200, 1500, 1700, 2000, 2300, 2600, and 3000 Kelvin.

First Pass CINDER code calculations for actinide buildup and depletion and associated fission product absorption are in progress.

IV. COMPARISON OF MONTE CARLO AND S_n CALCULATIONS WITH ^7Li PULSED SPHERE EXPERIMENTS USING ENDF/B-IV DATA (W. A. Reupke [Georgia Tech] and D. W. Muir)

As a test of nuclear data and methods, the neutron leakage fluence for a 0.5 mean-free-path ^7Li sphere pulsed with 14-MeV neutrons[45] was calculated with one-dimensional discrete ordinates and pointwise Monte Carlo particle transport codes using ENDF/B-IV data.

The pulsed-sphere problem specification[46] was modified to include the steel corrosion encapsulation because the encapsulation was not present in the target-out or blank run.[47] Preliminary calculations demonstrated that omission of the

encapsulation leads to 2, -3, and -8% change in leakage fluence, integrated over energy bands 15-10, 10-5, and 5-2 MeV, compared to the case with encapsulation included.

The one-dimensional discrete ordinates calculation was performed with the DTF code[48] using ENDF/B-IV cross sections processed into multigroup form by the NJOY code.[49] Energy boundaries corresponded to the GAM-II 100-group structure, within-group flux-weighting was flat, the dilution factor was infinite, and P_0 through P_5 Legendre moments were generated. A one-dimensional problem specification was obtained by transforming the experimental quasi-sphere into a system of concentric spherical shells in which the volumes and densities were adjusted to preserve the masses and the average radial positions of the original components. Spatial mesh interval was 0.5 cm, well below characteristic mean-free-path lengths, and the order of angular quadrature was 16. Execution time on the LASL CDC 7600 was two minutes.

The Monte Carlo calculations were implemented with the continuous-energy code MCN[50] using pointwise cross sections processed from ENDF/B-IV by R. J. LaBauve and D. George (see Sec. II B). A time-dependent energy-angle- and intensity-angle-correlated neutron source function and relativistic energy correction as developed by LASL Group TD-6 were used in the calculations. The neutron spectrum at a point detector 765 cm from the sphere center was binned into 0.2-MeV energy intervals, and represented neutrons accumulated at flight times between 130 and 410 ns. Approximately 80 000 neutrons were started to give a typical standard deviation of 7-8% in a fluence energy bin. Execution time on the LASL CDC 7600 was 15 minutes. The results of the calculations, converted to compatible units are compared with experiment in Fig. 11. While general agreement between both calculated spectra and the experimental spectrum is found, discrepancies of up to 40% are observed in some regions below the elastic peak. These discrepancies may be due to ENDF/B-IV data, to the data processing calculations, to the neutron transport calculations, to the conversion from experimental time-of-flight (TOF) data to energy spectrum data, or to an unknown experimental factor.

Discrepancies common to both calculations tend to rule out inadequacies in the two data processing procedures and in the neutron transport calculation. In particular, the over-prediction in the region 10-12 MeV, where calculation-to-experiment ratios (C/E) are as high as 1.4, and the under-prediction in the tail below 4 MeV, where C/E values are as low as 0.7, suggest a problem either in

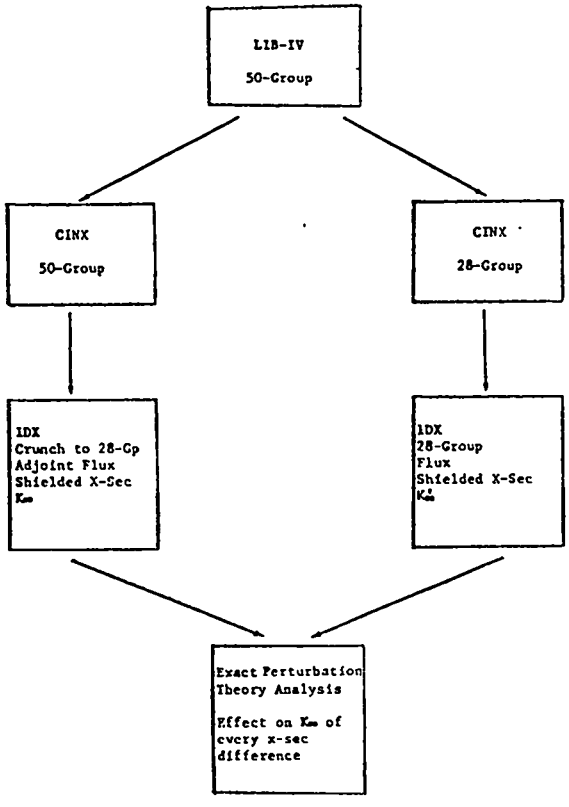

Fig. 10
Procedure for determining spectra effects in group collapsing.

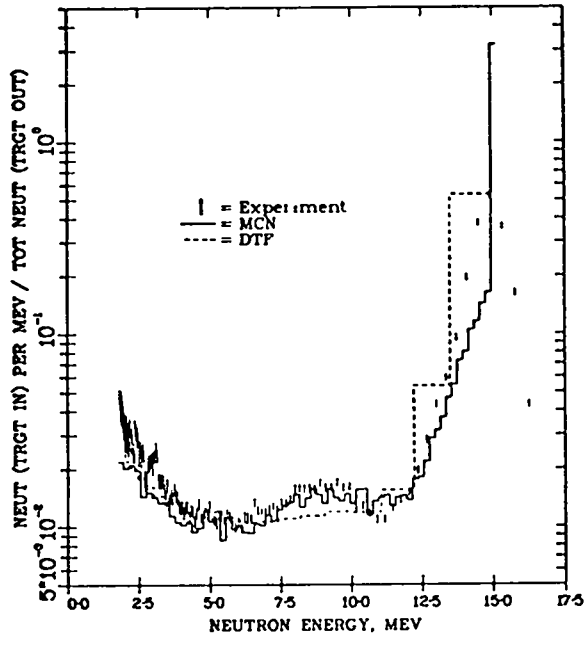

Fig. 11
Comparison of Monte Carlo and S_n calculations with 0.5 m.f.p. ^7Li pulsed sphere experiment.

the ENDF/B data, in the experiment definition, or in the conversion from TOF data to energy spectrum data. On the other hand, discrepancies limited to a particular transport calculation tend to implicate the corresponding data processing code or the transport calculation itself, as in the region 6-10 MeV, where multigroup discrete-ordinates under-predict both the experimental and Monte Carlo data by up to 30%.

By additional calculation, the sources of discrepancy may be further narrowed. For example, a previous C/E comparison of direct TOF results using a different Monte Carlo code[51] shows the same low-energy discrepancy. This suggests that the discrepancy in the low-energy tail is not due to the conversion from TOF data to energy spectrum data, but should be attributed to the ENDF/B data, or to a difficulty in the experiment definition. In another test, simulation of the discrete-ordinates results with a calculation of the one-dimensional model by Monte Carlo gives 2% agreement in the region 6-10 MeV. This result

suggests that the 30% discrepancy between 1D discrete ordinates and 2D Monte Carlo lies neither in the data processing stages nor in the discretization of neutron transport, but is attributable to the essential two-dimensional nature of the experimental neutron source and target sphere.

Appreciation is extended to J. Kammerdiener of Group TD-2 for helpful discussions of the sphere experiments, and to R. Schrandt, B. McArdle, R. Seamon, and J. MacDonald of Group TD-6 for assistance with various aspects of the MCN calculation.

V. FISSION-PRODUCT AND DECAY STUDIES

A. ENDF/B Phenomenological Yield Model Improvements (D. G. Madland and T. R. England)

1. Distribution of Independent Fission-Product Yields to Isomeric States.

Approximately 15% of the primary fission products in fission of actinide nuclei are nuclides which have an isomeric state with a half-life $\tau \geqslant 0.1$.[52] A simple semiempirical formalism is described for calculating the distribution of the independent yield strength, IY, between the ground and isomeric states in these cases. The calculated branching ratios are easily incorporated into the phenomenological (Gaussian) yield model to be used in Version V of ENDF/B. Previously (ENDF/B-IV), most yield branching ratios were set equal to 1 for expediency.[53]

It is assumed that (a) primary fragments are formed with a distribution, P(J), of total angular momentum, J, which is cut off at some characteristic value, $J_{rms} = \langle J^2 \rangle^{1/2}$, and (b) the primary branching mechanism is, simply, that fragments with J values close to that of the isomeric state (J_m) decay to the isomeric state, and framents with J values close to the ground state (J_g) decay to the ground state, the driving force being that electromagnetic transition rates are generally strongest for minimum ΔJ.

The form of the fragment angular momentum distribution used is that of Rasmussen[54]

$$P(J) \simeq (2J+1) \exp(-[J+1/2]^2/\langle J^2 \rangle) \quad . \tag{18}$$

Consider, for example, the case with A odd (all spins half-integer), $J_m > J_g$, and $|J_m - J_g|$ = odd integer. Then one finds

$$\frac{IY(\text{isomeric state})}{IY(\text{g.s.}) + IY(\text{isomeric state})} = \frac{\int_{(J_m+J_g+1)/2}^{\infty} P(J)dJ}{\int_{1/2}^{\infty} P(J)dj} \quad . \tag{19}$$

All together there are eight such cases depending on whether A and $|J_m - J_g|$ are even or odd, and whether J_m is greater or less than J_g. The resulting branching ratios, defined by R = IY (isomeric state/IY(g.s.)), are given in Table XI and are calculated with Eqs. (20)-(23)

$$F_1 = \exp(1/\langle J^2\rangle)\left\{\exp\left[-(1/\langle J^2\rangle)\left(\frac{J_m+J_g+3}{2}\right)^2\right]\right.$$
$$\left. + (1/\langle J^2\rangle)\left(\frac{J_m+J_g+1}{2}\right)\exp\left[-(1/\langle J^2\rangle)\left(\frac{J_m+J_g+1}{2}\right)^2\right]\right\} \quad , \tag{20}$$

$$F_2 = \exp(1/\langle J^2\rangle)\left\{\exp\left[-(1/\langle J^2\rangle)\left(\frac{J_m+J_g+2}{2}\right)^2\right]\right\} \quad , \tag{21}$$

$$F_3 = \exp\left[-(1/\langle J^2\rangle)\left(\frac{J_m+J_g+2}{2}\right)\left(\frac{J_m+J_g+4}{2}\right)\right]$$
$$+ (1/\langle J^2\rangle)\left(\frac{J_m+J_g+1}{2}\right)\exp\left[-(1/\langle J^2\rangle)\left(\frac{J_m+J_g}{2}\right)\left(\frac{J_m+J_g+2}{2}\right)\right] \quad , \tag{22}$$

$$F_4 = \exp\left[-(1/\langle J^2\rangle)\left(\frac{J_m+J_g+1}{2}\right)\left(\frac{J_m+J_g+3}{2}\right)\right] \quad . \tag{23}$$

TABLE XI

INDEPENDENT YIELD BRANCHING RATIOS,
R, FOR ISOMERIC STATES

ODD A

$J_m - J_g$ = even integer $J_m > J_g$ $\left(\frac{F_1}{1 - F_1}\right)$	$J_m - J_g$ = even integer $J_m < J_g$ $\left(\frac{1 - F_1}{F_1}\right)$
$J_m - J_g$ = odd integer $J_m > J_g$ $\left(\frac{F_2}{1 - F_2}\right)$	$J_m - J_g$ = odd integer $J_m < J_g$ $\left(\frac{1 - F_2}{F_2}\right)$

EVEN A

$J_m - J_g$ = even integer $J_m > J_g$ $\left(\frac{F_3}{1 - F_3}\right)$	$J_m - J_g$ = even integer $J_m < J_g$ $\left(\frac{1 - F_3}{F_3}\right)$
$J_m - J_g$ = odd integer $J_m > J_g$ $\left(\frac{F_4}{1 - F_4}\right)$	$J_m - J_g$ = odd integer $J_m < J_g$ $\left(\frac{1 - F_4}{F_4}\right)$

J_{rms} values were presumed energy dependent[55] and were determined empirically as a function of neutron energy with the result that J_{rms} = (7.5, 7.5, 8.0, 9.0, and 10.0) for E_n(MeV) = (thermal, 0.5, 2.0, 10.0, and 14.0), respectively.

Comparisons of calculated and experimental[56-59] results are shown in Fig. 12. A total of 423 cases at 3 neutron energies has been calculated. A detailed LASL report on the calculations has been prepared and will be published soon tENDF-241). Where experimental data do not exist, the calculated results have been recommended for the expanded ENDF/B-V fission yields.

2. Pairing Effects on the Distribution of Fission-Product Yields. Version V of ENDF/B is expected to have > 20 yield sets for > 13 fissionable nuclides applicable at one or more fission neutron energies; the effects of neutron and proton pairing are needed. To date the Z pairing effects, based on assessments of measured yields, have been reported for ^{233}U, ^{235}U, and ^{239}Pu at thermal energies.[60-63] For ^{233}U and ^{235}U, N and Z pairing effects for thermal fission and the Z pairing effect for fast fission have been reported.[61] Experimental data for other fissionable nuclides and energies are, at present, inadequate for similar analyses.

For use in ENDF/B-V, we have developed semiempirical relations for the average Z pairing effect based on a correlation with the excitation energy of the compound system relative to the outer fission barrier; to first order, the smaller N pairing effect is proportional to the Z pairing. The relations can be incorporated into the phenomenological model used in ENDF/B for isobaric yield distributions.[53] The results, based on ^{235}U yield data[53,61,64] and measured barrier heights,[65-67] predict pairing effects for other even-even compound systems in good agreement with experimental analyses.

There are four factors, F_i, which modulate the normal independent yields (NIY), i.e., for each mass chain nuclide the independent yield is (IY) = F_i(NIY) where

$$F_i = 1 \pm X \pm Y \quad .$$

Here X(Y) is the proton (neutron) pairing enhancement relative to the normal yield, i refers to nuclide type (even-even, even-odd, etc.), and the + sign is used for an even number of nucleons. Except for prompt neutron emission, X and Y would likely be equal but, in fact, X is about five times larger than Y (averaged over all masses) which explains the usual reference to the *even-odd* Z *effect*.

Figure 13, which illustrates the values of (F_i-1) extracted from ^{235}U thermal fission data, clearly demonstrates the existence of four factors; the neutron pairing effect is obviously stronger for the heavy mass region.

Table XII lists selected results for 11 nuclides at 4 fission neutron energies (tabulated values represent pairing effects averaged over the entire fission product mass range). At 14 MeV, average X and Y values are 0.015 ± 0.015 and 0.003 ± 0.003, respectively. (The large uncertainties reflect the paucity of 14-MeV data.) For odd-Z systems, such as ^{241}Am and ^{243}Am, the X value is expected to be zero. The complete calculation is described in detail in Ref. 68.

The calculated results have been recommended for use in the phenomenological yield model for the ENDF/B-V fission products in the absence of experimental data.

B. Fission Yield Theory: Statistical Model Development (D. G. Madland, R. F. Pepping [University of Wisconsin], C. W. Maynard [University of Wisconsin], T. R. England, and P. G. Young)

Work is progressing on the initial version of a statistical model calculation of fission product yields for ^{235}U thermal-neutron-induced fission. This case has been chosen to test model developments because it has been studied experimentally more than any other fissionable nuclide.

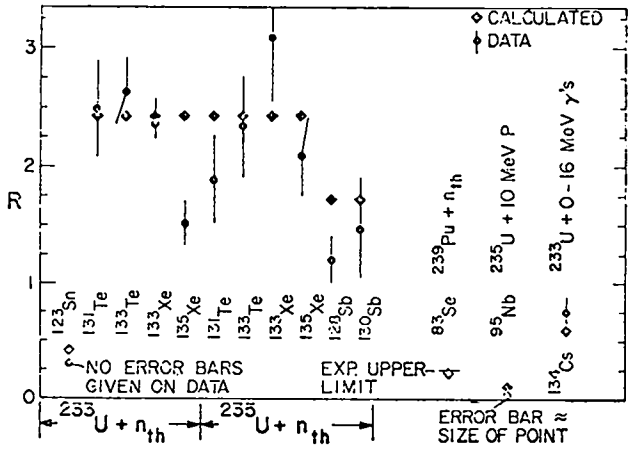

Fig. 12
Comparisons of calculated and experimental branching ratios R for isomeric states

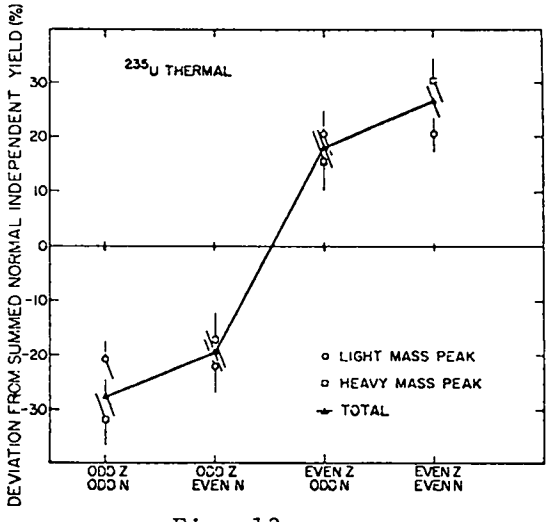

Fig. 13
Deviation of the summed IY from the summed NIY for odd-odd, odd-even, even-odd, and even-even fission products and for the light mass peak, heavy mass peak, and the total mass distribution in ^{235}U thermal.

TABLE XII

ESTIMATED VALUES OF X AT FOUR NEUTRON FISSION ENERGIES[a]

Fission Target	0.0 MeV	0.5 MeV	1.0 MeV	2 MeV
^{232}Th	-----	-----	-----	$0.33^{+0.54}_{-0.33}$
^{233}U	$0.21^{+0.29}_{-0.21}$(b)	$0.14^{+0.18}_{-0.14}$	$0.11^{+0.13}_{-0.11}$	$0.07^{+0.09}_{-0.07}$(b)
^{234}U	-----	$0.67^{+1.83}_{-0.67}$	$0.27^{+0.41}_{-0.27}$	$0.12^{+0.15}_{-0.12}$
^{235}U	0.228±0.034(c)	$0.15^{+0.19}_{-0.15}$	$0.11^{+0.14}_{-0.11}$	0.078±0.063(c)
^{236}U	-----	-----	$0.63^{+1.67}_{-0.63}$	$0.17^{+0.22}_{-0.17}$
^{238}U	-----	-----	-----	$0.33^{+0.55}_{-0.33}$
^{238}Pu	$0.46^{+0.96}_{-0.46}$	$0.23^{+0.33}_{-0.23}$	$0.15^{+0.19}_{-0.15}$	$0.09^{+0.11}_{-0.09}$
^{239}Pu	$0.17^{+0.22}_{-0.17}$	$0.12^{+0.15}_{-0.12}$	$0.10^{+0.12}_{-0.10}$	$0.07^{+0.08}_{-0.07}$
^{240}Pu	-----	$0.53^{+1.23}_{-0.53}$	$0.24^{+0.36}_{-0.24}$	$0.12^{+0.14}_{-0.12}$
^{241}Pu	$0.21^{+0.28}_{-0.21}$	$0.14^{+0.18}_{-0.14}$	$0.11^{+0.13}_{-0.11}$	$0.07^{+0.09}_{-0.07}$
^{242}Pu	-----	-----	$0.36^{+0.65}_{-0.36}$	$0.14^{+0.18}_{-0.14}$

[a] Uncertainties for all nuclides are based upon uncertainties in model parameters; Y values are given by $Y=\alpha X$, where $\alpha=0.193 \pm 0.152$ from an analysis of ^{235}U thermal and fast fission data.

b ^{233}U values are in excellent agreement with the results from data evaluations (which show much smaller uncertainties).

c ^{235}U values derived from experimental data; used to determine model parameters.

Coding has begun on the calculation of deformation energies of the primary fission fragments, based upon the binding energy optimization procedure given by Seegar and Howard.[69] The extracted deformation energies will be used in a representation of the excitation energy of the primary fragment. The total excitation energy is one of three major terms used in the argument of the statistical level density expression. The next steps will be to (a) incorporate the residual mass (difference between measured and calculated[69] mass) into the expression for the fragment binding energy and (b) to perform an extrapolation on the residuals into regions where they are unknown.

C. Calculation vs Experiment: Comparisons of Time-Dependent β^- and γ Spectra From Thermal Fission of ^{235}U (T. R. England and M. G. Stamatelatos)

Beta and gamma energies and intensities for the 181 nuclides with spectral data in ENDF/B-IV have been used to produce several libraries of group spectra. One library contains 150 gamma groups (constant 50-keV width from 0 to 7.5 MeV) and 75 beta groups (constant 100 keV width from 0 to 7.5 MeV). A corresponding 150-group gamma library was generated for use in comparing CINDER-10 calculations with preliminary unpublished gamma spectral measurements by E. Jurney (LASL P-DO) by folding in the detector energy resolution.

Table XIII provides a comparison of the integrated energy release rates at the four average cooling times analyzed to date. Some fraction of the conversion electron energy should be excluded from such comparisons. In these comparisons only the conversion electron energy for the 38 nuclides having specified conversion fractions in ENDF/B-IV is excluded; Table XIII shows the comparison with and without this exclusion.

There are 711 unstable nuclides in the calculation of total decay energies. The last column shows the percent contribution to the total gamma energy release rate due to the 181 nuclides.

Comparisons of the absolute gamma spectra are shown in Figs. 14-17. The spectral comparisons were normalized to the total calculated energy to account for the contribution of the remaining 530 isotopes for which spectral data do not exist in ENDF/B-IV. The measured and calculated spectra used an irradiation time of 20 000 s.

The calculated beta energy release rate is compared in Table XIV with experimental values from Ref. 70. Calculation and experiment are based on an irradiation time of 28 800 s. Except for the value at 6 s cooling, all values are well inside the experimental uncertainties (7 to 10%).

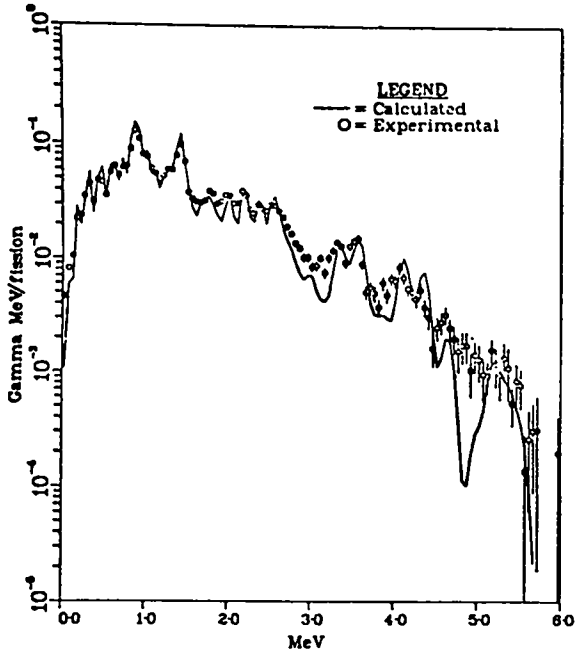

Fig. 14
Gamma spectrum 5.56 h irradiation, 70 s cooling.

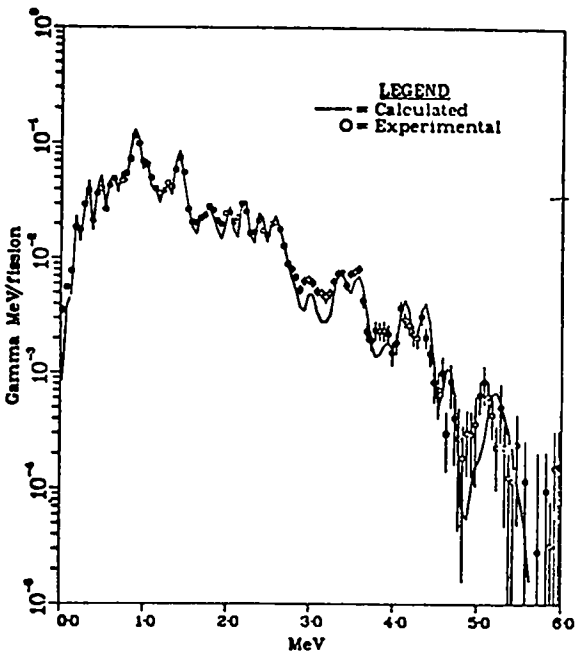

Fig. 15
Gamma spectrum, 5.56 h irradiation, 199 s cooling.

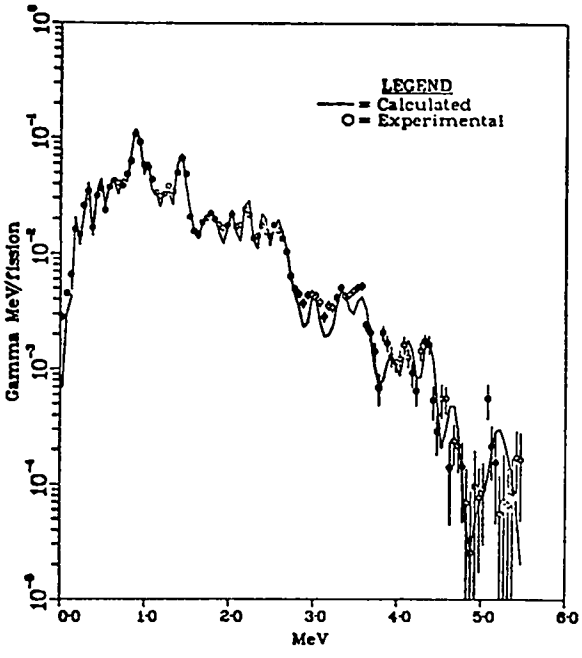

Fig. 16
Gamma spectrum, 5.56 h irradiation, 388 s cooling.

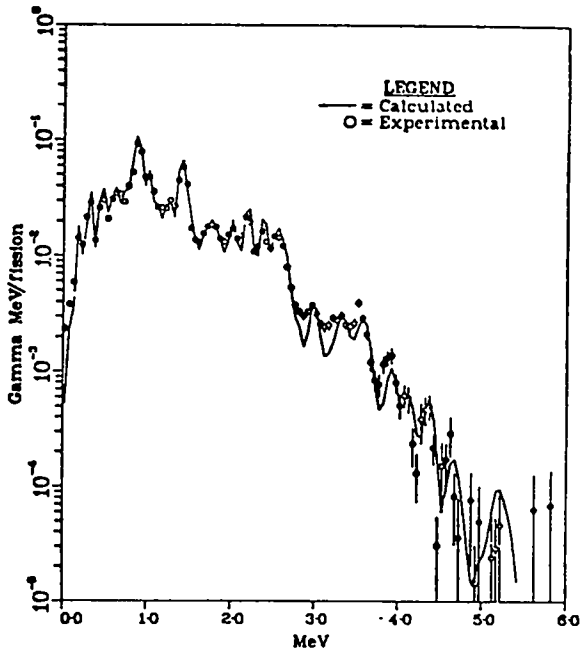

Fig. 17
Gamma spectrum, 5.56 h irradiation, 660 s cooling.

TABLE XIII

COMPARISON OF ENERGY INTEGRATED γ MeV/FISSION
(% deviation of calculation from experiment)

Cooling Times	% CAL-EXP / EXP: Including Conversion Electron	% CAL-EXP / EXP: Excluding Conversion Electron	% of Total γ MeV/F Due to Nuclides Having Spectra(181)
70	+ 0.3	+ 0.07	87.6
199	+ 1.5	+ 1.1	93.5
388	+ 1.3	+ 0.9	95.5
660	+ 5.1	+ 4.7	96.6

TABLE XIV

COMPARISON OF ENERGY INTEGRATED β MeV/FISSION
(% deviation of calculation from experiment)

COOLING TIME	% CAL-EXP / EXP
6s	- 13.8
21s	- 4.9
66s	- 3.2
3750s	+ 3.4
10,950s	+ 6.0

Figures 18-22 show the actual β^- spectral comparisons. In the gamma and beta comparisons, we have chosen to plot the energy relase rate (in units of MeV/fis/bin) rather than multiplicities. This emphasizes the spectra at high energies where we also see the largest departure of calculation from experiment. The data library used in the calculations is described in Ref. 52.

D. Noble Gases, Halogens, and Other Fission Products (T. R. England and N. L. Whittemore)

A large number of CINDER-10 calculations using ENDF/B-IV data are in progress to determine various source terms for use in studies of spent or irradiated fuel accidents. These include the content, absorption, beta and gamma energy, and corresponding spectra for halogens, noble gases, and the total fission-pro-

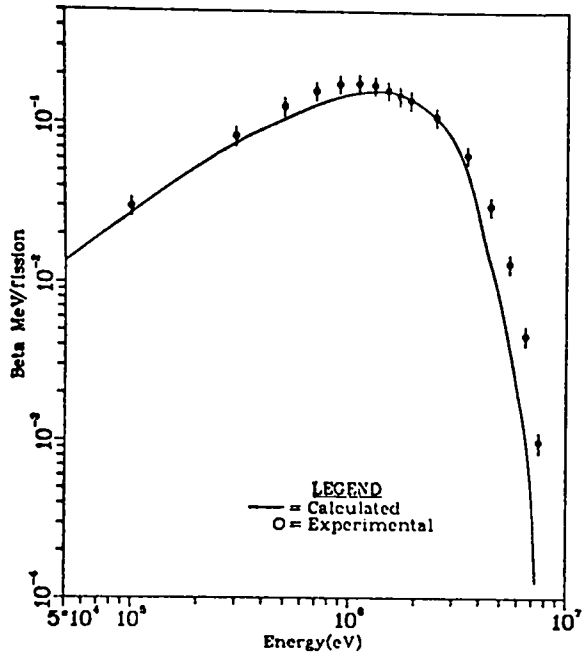

Fig. 18
Beta MeV/fis at 8 h irradiation and 6 s decay.

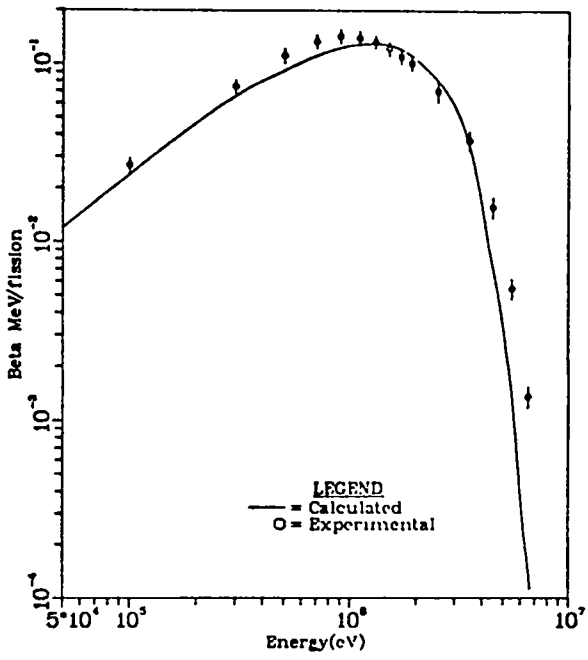

Fig. 19
Beta MeV/fis at 8 h irradiation and 21 s decay.

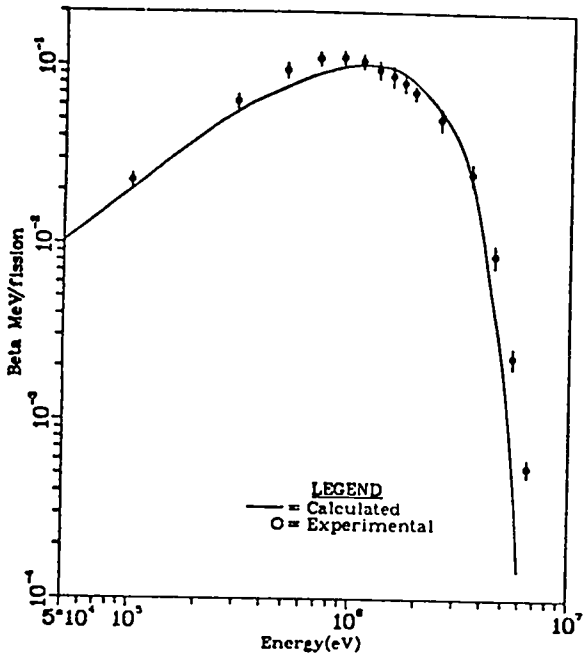

Fig. 20
Beta MeV/fis at 8 h irradiation and 66 s decay.

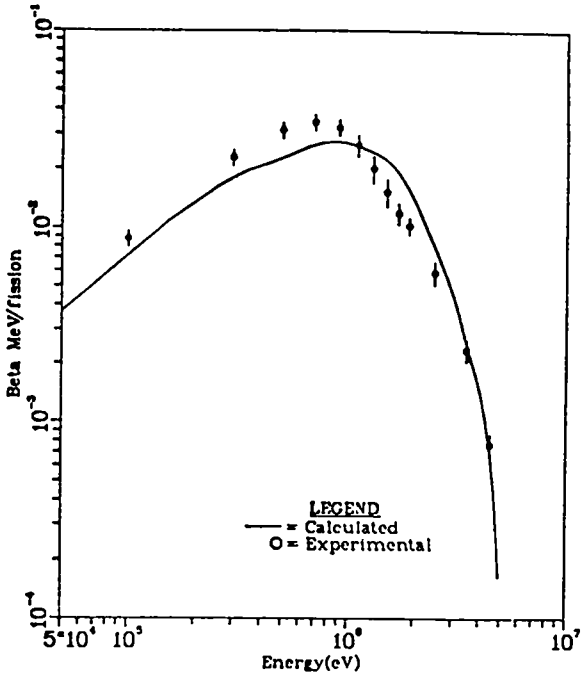

Fig. 21
Beta MeV/fis at 8 h irradiation and 3750 s decay.

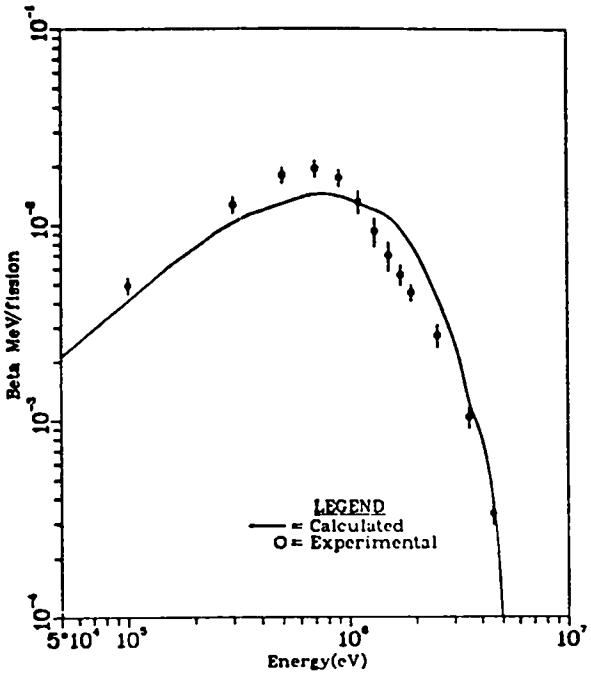

Fig. 22.
Beta MeV/fis at 8 h irradiation and 9576 s decay.

duct ensemble. In addition, calculations of halogens and noble gases and their progeny (subsequent to a partial or complete escape of these gases) are in progress for use in radiolyses and synergistic studies. The calculations include the 824 nuclides in the ENDF/B-IV fission product files.[52] Of these, there are 93 gaseous isotopes of Kr, Br, I, and Xe, with 78 being radioactive.

Fission burst calculations for those fissionable nuclides having yield data in ENDF/B-IV have been completed. These results can, with additional effort, be used to generate a burst kernel which can be folded into any power history if neutron absorption can be ignored (as in the current ANS 5.1 Decay Heat Standard).

Calculations for the infinite irradiation of ^{235}U where absorption in fission products is ignored have also been carried out. This type calculation is equivalent to a fission burst in that one can be derived from the other. In addition, the case of a finite irradiation without absorption can be derived from either type of calculation.

Of more immediate use, calculations for typical reactor lifetimes and power histories where neutron absorption is permitted are in progress. Currently, these calculations use four-group cross sections.

Tables XV-XXIII show aggregate summary results for the case of ^{235}U thermal fission for one year at a constant fission rate and constant flux. The thermal

TABLE XV

BARNS/FISSION DURING AND FOLLOWING $^{235}U + n_{th}$ FISSION
WITH ALL FISSION PRODUCTS INCLUDED

Time Step	Elapsed Time (s)	barns / fiss			
		Group I	Group II	Group III	Group IV
1	6.2208E+06	4.9325E-02	2.3129E-01	1.8012E+01	8.7176E+02
2	1.2442E+07	5.0116E-02	2.3511E-01	1.8534E+01	4.7272E+02
3	1.8662E+07	5.0407E-02	2.3638E-01	1.8656E+01	3.3698E+02
4	2.4883E+07	5.0577E-02	2.3678E-01	1.8612E+01	2.6777E+02
5	3.1104E+07	5.0702E-02	2.3680E-01	1.8487E+01	2.2550E+02
6	3.1104E+07	5.0702E-02	2.3680E-01	1.8487E+01	2.2550E+02
7	3.1104E+07	5.0702E-02	2.3680E-01	1.8487E+01	2.2550E+02
8	3.1104E+07	5.0702E-02	2.3680E-01	1.8487E+01	2.2550E+02
9	3.1104E+07	5.0702E-02	2.3680E-01	1.8487E+01	2.2551E+02
10	3.1104E+07	5.0702E-02	2.3680E-01	1.8487E+01	2.2553E+02
11	3.1104E+07	5.0702E-02	2.3680E-01	1.8487E+01	2.2557E+02
12	3.1104E+07	5.0702E-02	2.3680E-01	1.8487E+01	2.2568E+02
13	3.1104E+07	5.0702E-02	2.3680E-01	1.8487E+01	2.2587E+02
14	3.1104E+07	5.0702E-02	2.3680E-01	1.8488E+01	2.2623E+02
15	3.1104E+07	5.0702E-02	2.3680E-01	1.8488E+01	2.2731E+02
16	3.1105E+07	5.0703E-02	2.3680E-01	1.8488E+01	2.2905E+02
17	3.1106E+07	5.0704E-02	2.3681E-01	1.8489E+01	2.3231E+02
18	3.1109E+07	5.0706E-02	2.3682E-01	1.8491E+01	2.4064E+02
19	3.1114E+07	5.0709E-02	2.3684E-01	1.8494E+01	2.5044E+02
20	3.1124E+07	5.0714E-02	2.3687E-01	1.8497E+01	2.5838E+02
21	3.1154E+07	5.0724E-02	2.3694E-01	1.8498E+01	2.3468E+02
22	3.1204E+07	5.0736E-02	2.3703E-01	1.8494E+01	1.7047E+02
23	3.1304E+07	5.0754E-02	2.3718E-01	1.8494E+01	1.1652E+02
24	3.1604E+07	5.0801E-02	2.3752E-01	1.8519E+01	1.0850E+02
25	3.2104E+07	5.0864E-02	2.3792E-01	1.8566E+01	1.0953E+02
26	3.3104E+07	5.0944E-02	2.3844E-01	1.8648E+01	1.0931E+02
27	3.6104E+07	5.1051E-02	2.3924E-01	1.8794E+01	1.0827E+02
28	4.1104E+07	5.1151E-02	2.3987E-01	1.8875E+01	1.0737E+02
29	5.1104E+07	5.1316E-02	2.4026E-01	1.8838E+01	1.0695E+02
30	8.1104E+07	5.1638E-02	2.4005E-01	1.8487E+01	1.0703E+02

TABLE XVI

ENERGY RELEASE RATES IN $^{235}U + n_{th}$ FISSION

WITH ALL FISSION PRODUCTS INCLUDED

Time Step	Cooling Time (s)	MeV/fis		
		Beta	Gamma	Total
1	0.	6.28870E+00	6.00881E+00	1.22975E+01
2	0.	6.32487E+00	6.04695E+00	1.23718E+01
3	0.	6.34551E+00	6.06585E+00	1.24114E+01
4	0.	6.35976E+00	6.07609E+00	1.24359E+01
5	0.	6.37073E+00	6.08202E+00	1.24527E+01
6	9.99982E-03	6.36155E+00	6.07504E+00	1.24366E+01
7	1.00000E+00	5.80535E+00	5.66059E+00	1.14659E+01
8	2.00000E+00	5.49999E+00	5.43899E+00	1.09390E+01
9	5.00000E+00	4.95944E+00	5.05419E+00	1.00136E+01
10	1.00000E+01	4.46457E+00	4.70236E+00	9.16693E+00
11	2.00000E+01	3.93103E+00	4.29688E+00	8.22791E+00
12	5.00000E+01	3.24463E+00	3.69909E+00	6.94372E+00
13	1.00000E+02	2.76328E+00	3.23511E+00	5.99839E+00
14	2.00000E+02	2.34289E+00	2.81344E+00	5.15633E+00
15	5.00000E+02	1.88386E+00	2.35770E+00	4.24157E+00
16	1.00000E+03	1.57556E+00	2.04058E+00	3.61613E+00
17	2.00000E+03	1.28515E+00	1.70177E+00	2.98693E+00
18	5.00000E+03	9.67499E-01	1.25068E+00	2.21818E+00
19	1.00000E+04	7.85922E-01	9.65772E-01	1.75169E+00
20	2.00000E+04	6.27915E-01	7.58400E-01	1.38632E+00
21	5.00000E+04	4.42586E-01	5.82027E-01	1.02461E+00
22	1.00000E+05	3.38616E-01	4.79899E-01	8.18516E-01
23	2.00000E+05	2.70304E-01	3.95293E-01	6.65597E-01
24	5.00000E+05	2.11898E-01	2.99207E-01	5.11105E-01
25	1.00000E+06	1.73337E-01	2.25817E-01	3.99154E-01
26	2.00000E+06	1.34600E-01	1.56407E-01	2.91006E-01
27	5.00000E+06	8.67027E-02	8.36024E-02	1.70305E-01
28	1.00000E+07	5.68440E-02	4.53015E-02	1.02145E-01
29	2.00000E+07	3.32274E-02	1.58114E-02	4.90388E-02
30	5.00000E+07	1.35562E-02	2.34088E-03	1.58971E-02

TABLE XVII

HALOGENS PLUS NOBLE GAS FRACTIONS IN $^{235}U + n_{th}$ FISSION.
(Listed values are fractions of all fission products)

Time Step	Cooling Time (s)	Density	Radioactive Density	Curies	Energy Release Rate: Beta	Gamma	Total
1	0.	1.3514E-01	1.172E-02	1.977E-01	2.0125E-01	2.4781E-01	2.2400E-01
2	0.	1.3338E-01	8.168E-03	1.938E-01	2.0011E-01	2.4626E-01	2.2267E-01
3	0.	1.3268E-01	7.000E-03	1.919E-01	1.9946E-01	2.4550E-01	2.2196E-01
4	0.	1.3224E-01	6.414E-03	1.908E-01	1.9901E-01	2.4510E-01	2.2153E-01
5	0.	1.3190E-01	6.059E-03	1.901E-01	1.9867E-01	2.4487E-01	2.2124E-01
6	9.9998E-03	1.3190E-01	6.059E-03	1.901E-01	1.9877E-01	2.4498E-01	2.2134E-01
7	1.0000E+00	1.3190E-01	6.059E-03	1.916E-01	2.0219E-01	2.4982E-01	2.2570E-01
8	2.0000E+00	1.3190E-01	6.059E-03	1.919E-01	2.0231E-01	2.5107E-01	2.2656E-01
9	5.0000E+00	1.3190E-01	6.059E-03	1.922E-01	2.0131E-01	2.5240E-01	2.2709E-01
10	1.0000E+01	1.3190E-01	6.059E-03	1.925E-01	1.9984E-01	2.5333E-01	2.2728E-01
11	2.0000E+01	1.3190E-01	6.059E-03	1.921E-01	1.9581E-01	2.5367E-01	2.2603E-01
12	5.0000E+01	1.3190E-01	6.059E-03	1.889E-01	1.8327E-01	2.5230E-01	2.2004E-01
13	1.0000E+02	1.3190E-01	6.058E-03	1.858E-01	1.7013E-01	2.5215E-01	2.1437E-01
14	2.0000E+02	1.3190E-01	6.058E-03	1.835E-01	1.5667E-01	2.5642E-01	2.1110E-01
15	5.0000E+02	1.3190E-01	6.057E-03	1.837E-01	1.4388E-01	2.7104E-01	2.1456E-01
16	1.0000E+03	1.3190E-01	6.055E-03	1.883E-01	1.4244E-01	2.9002E-01	2.2572E-01
17	2.0000E+03	1.3190E-01	6.052E-03	1.978E-01	1.5137E-01	3.1790E-01	2.4625E-01
18	5.0000E+03	1.3190E-01	6.043E-03	2.069E-01	1.5998E-01	3.5277E-01	2.6868E-01
19	1.0000E+04	1.3189E-01	6.029E-03	2.028E-01	1.5190E-01	3.4660E-01	2.5924E-01
20	2.0000E+04	1.3188E-01	6.004E-03	1.949E-01	1.4390E-01	3.1680E-01	2.3848E-01
21	5.0000E+04	1.3185E-01	5.939E-03	1.857E-01	1.4919E-01	2.8260E-01	2.2497E-01
22	1.0000E+05	1.3181E-01	5.847E-03	1.701E-01	1.3876E-01	2.5013E-01	2.0406E-01
23	2.0000E+05	1.3175E-01	5.693E-03	1.477E-01	1.1098E-01	2.1040E-01	1.7003E-01
24	5.0000E+05	1.3160E-01	5.345E-03	1.087E-01	6.8481E-02	1.3313E-01	1.0633E-01
25	1.0000E+06	1.3143E-01	4.994E-03	6.408E-02	3.4853E-02	6.3092E-02	5.0829E-02
26	2.0000E+06	1.3129E-01	4.724E-03	2.164E-02	1.0413E-02	1.6806E-02	1.3849E-02
27	5.0000E+06	1.3128E-01	4.639E-03	1.661E-03	9.6136E-04	1.0125E-03	9.8646E-04
28	1.0000E+07	1.3130E-01	4.645E-03	1.088E-03	7.2811E-04	2.2105E-05	4.1500E-04
29	2.0000E+07	1.3130E-01	4.628E-03	2.198E-03	1.2129E-03	2.2694E-05	8.2916E-04
30	5.0000E+07	1.3123E-01	4.552E-03	5.737E-03	2.7959E-03	1.4409E-04	2.4054E-03

TABLE XVIII

NOBLE GAS FRACTIONS IN $^{235}U + n_{th}$ FISSION

(The listed values are fractions of all fission products)

Time Step	Cooling Time (s)	Density	Radioactive Density	Curies	Energy Release Rate		
					Beta	Gamma	Total
1	0.	1.2746E-01	5.634E-03	1.038E-01	9.9277E-02	9.5896E-02	9.7625E-02
2	0.	1.2707E-01	3.498E-03	1.017E-01	9.8711E-02	9.5291E-02	9.7039E-02
3	0.	1.2681E-01	2.780E-03	1.007E-01	9.8391E-02	9.4994E-02	9.6731E-02
4	0.	1.2658E-01	2.417E-03	1.001E-01	9.8172E-02	9.4834E-02	9.6541E-02
5	0.	1.2637E-01	2.197E-03	9.975E-02	9.8004E-02	9.4742E-02	9.6411E-02
6	9.9998E-03	1.2637E-01	2.197E-03	9.976E-02	9.8050E-02	9.4769E-02	9.6447E-02
7	1.0000E+00	1.2637E-01	2.197E-03	1.004E-01	1.0027E-01	9.6014E-02	9.8167E-02
8	2.0000E+00	1.2637E-01	2.197E-03	1.006E-01	1.0079E-01	9.6263E-02	9.8539E-02
9	5.0000E+00	1.2637E-01	2.197E-03	1.006E-01	1.0126E-01	9.6457E-02	9.8837E-02
10	1.0000E+01	1.2637E-01	2.196E-03	1.007E-01	1.0174E-01	9.6627E-02	9.9115E-02
11	2.0000E+01	1.2637E-01	2.196E-03	1.000E-01	1.0098E-01	9.5810E-02	9.8280E-02
12	5.0000E+01	1.2637E-01	2.196E-03	9.727E-02	9.6371E-02	9.2166E-02	9.4131E-02
13	1.0000E+02	1.2637E-01	2.196E-03	9.458E-02	9.0588E-02	8.9003E-02	8.9733E-02
14	2.0000E+02	1.2637E-01	2.196E-03	9.160E-02	8.2076E-02	8.6184E-02	8.4318E-02
15	5.0000E+02	1.2637E-01	2.195E-03	8.613E-02	6.4850E-02	7.9743E-02	7.3128E-02
16	1.0000E+03	1.2637E-01	2.195E-03	8.286E-02	5.2109E-02	7.4387E-02	6.4681E-02
17	2.0000E+03	1.2637E-01	2.194E-03	8.310E-02	4.6888E-02	7.2012E-02	6.1202E-02
18	5.0000E+03	1.2637E-01	2.192E-03	8.621E-02	4.3411E-02	7.2093E-02	5.9583E-02
19	1.0000E+04	1.2638E-01	2.190E-03	8.819E-02	3.9573E-02	6.9301E-02	5.5963E-02
20	2.0000E+04	1.2639E-01	2.187E-03	8.874E-02	3.6354E-02	5.5860E-02	4.7025E-02
21	5.0000E+04	1.2641E-01	2.170E-03	8.907E-02	3.7543E-02	3.4084E-02	3.5578E-02
22	1.0000E+05	1.2642E-01	2.132E-03	8.597E-02	3.3710E-02	2.5221E-02	2.8733E-02
23	2.0000E+05	1.2643E-01	2.047E-03	7.977E-02	2.5915E-02	1.9106E-02	2.1871E-02
24	5.0000E+05	1.2638E-01	1.811E-03	6.445E-02	2.0263E-02	1.3879E-02	1.6526E-02
25	1.0000E+06	1.2631E-01	1.566E-03	3.807E-02	1.2171E-02	7.9688E-03	9.7935E-03
26	2.0000E+06	1.2627E-01	1.389E-03	1.145E-02	3.7385E-03	2.4785E-03	3.0613E-03
27	5.0000E+06	1.2628E-01	1.330E-03	8.911E-04	5.3572E-04	8.3557E-05	3.1375E-04
28	1.0000E+07	1.2627E-01	1.316E-03	1.079E-03	7.2370E-04	1.0484E-05	4.0739E-04
29	2.0000E+07	1.2624E-01	1.289E-03	2.198E-03	1.2129E-03	2.2691E-05	8.2916E-04
30	5.0000E+07	1.2617E-01	1.212E-03	5.737E-03	2.7959E-03	1.4409E-04	2.4054E-03

TABLE XIX

INTEGRATED ENERGY VS COOLING TIME IN $^{235}U + n_{th}$ FISSION WITH ALL FISSION PRODUCTS INCLUDED

Time Step	Cooling Time (s)	MeV Beta	MeV Gamma	MeV Total
6	1.0000E-02	6.3661E-02	6.0785E-02	1.2445E-01
7	1.0000E+00	5.9218E+00	5.7479E+00	1.1670E+01
8	2.0000E+00	1.1556E+01	1.1284E+01	2.2840E+01
9	5.0000E+00	2.7109E+01	2.6930E+01	5.4039E+01
10	1.0000E+01	5.0506E+01	5.1210E+01	1.0172E+02
11	2.0000E+01	9.2122E+01	9.5944E+01	1.8807E+02
12	5.0000E+01	1.9788E+02	2.1431E+02	4.1219E+02
13	1.0000E+02	3.4638E+02	3.8608E+02	7.3246E+02
14	2.0000E+02	5.9871E+02	6.8561E+02	1.2843E+03
15	5.0000E+02	1.2199E+03	1.4490E+03	2.6689E+03
16	1.0000E+03	2.0736E+03	2.5376E+03	4.6112E+03
17	2.0000E+03	3.4825E+03	4.3843E+03	7.8668E+03
18	5.0000E+03	6.7676E+03	8.6770E+03	1.5445E+04
19	1.0000E+04	1.1084E+04	1.4106E+04	2.5190E+04
20	2.0000E+04	1.8033E+04	2.2567E+04	4.0600E+04
21	5.0000E+04	3.3513E+04	4.2160E+04	7.5673E+04
22	1.0000E+05	5.2631E+04	6.8335E+04	1.2097E+05
23	2.0000E+05	8.2558E+04	1.1147E+05	1.9403E+05
24	5.0000E+05	1.5322E+05	2.1282E+05	3.6604E+05
25	1.0000E+06	2.4810E+05	3.4113E+05	5.8923E+05
26	2.0000E+06	3.9905E+05	5.2617E+05	9.2521E+05
27	5.0000E+06	7.1504E+05	8.5867E+05	1.5737E+06
28	1.0000E+07	1.0602E+06	1.1604E+06	2.2206E+06
29	2.0000E+07	1.4866E+06	1.4241E+06	2.9108E+06
30	5.0000E+07	2.1016E+06	1.6078E+06	3.7094E+06

TABLE XX

HALOGENS AND PROGENY VS COOLING TIME FOR $^{235}U + n_{th}$ FISSION[a]

Time Step	Cooling Time (s)	Density	Activity	Mev/Fis Beta	Gamma	Total
6	9.99982E-03	1.05267E-06	1.63861E+12	6.40704E-01	9.12531E-01	1.55323E+00
7	1.00000E+00	1.05267E-06	1.57894E+12	5.88530E-01	8.68328E-01	1.45686E+00
8	2.00000E+00	1.05267E-06	1.53641E+12	5.52453E-01	8.37812E-01	1.39027E+00
9	5.00000E+00	1.05267E-06	1.45295E+12	4.84639E-01	7.79762E-01	1.26440E+00
10	1.00000E+01	1.05267E-06	1.37147E+12	4.22472E-01	7.24685E-01	1.14716E+00
11	2.00000E+01	1.05267E-06	1.27981E+12	3.57368E-01	6.63818E-01	1.02119E+00
12	5.00000E+01	1.05267E-06	1.14896E+12	2.73233E-01	5.78563E-01	8.51795E-01
13	1.00000E+02	1.05267E-06	1.05046E+12	2.15638E-01	5.16027E-01	7.31665E-01
14	2.00000E+02	1.05267E-06	9.70264E+11	1.72648E-01	4.67772E-01	6.40420E-01
15	5.00000E+02	1.05267E-06	9.04606E+11	1.44159E-01	4.30935E-01	5.75094E-01
16	1.00000E+03	1.05267E-06	8.66389E+11	1.32471E-01	4.04072E-01	5.36543E-01
17	2.00000E+03	1.05268E-06	8.13164E+11	1.18377E-01	3.60017E-01	4.78394E-01
18	5.00000E+03	1.05270E-06	6.96119E+11	9.14441E-02	2.67517E-01	3.58961E-01
19	1.00000E+04	1.05273E-06	5.86422E+11	6.96706E-02	1.87502E-01	2.57172E-01
20	2.00000E+04	1.05279E-06	4.84221E+11	5.29474E-02	1.23815E-01	1.76762E-01
21	5.00000E+04	1.05293E-06	3.48994E+11	3.52657E-02	6.58669E-02	1.01133E-01
22	1.00000E+05	1.05310E-06	2.35307E+11	2.13413E-02	3.53036E-02	5.66449E-02
23	2.00000E+05	1.05327E-06	1.42583E+11	1.01640E-02	1.73978E-02	2.75618E-02
24	5.00000E+05	1.05336E-06	7.89225E+10	4.10354E-03	7.88236E-03	1.19859E-02
25	1.00000E+06	1.05335E-06	4.34965E+10	2.26987E-03	4.39004E-03	6.65990E-03
26	2.00000E+06	1.05333E-06	1.44809E+10	7.89775E-04	1.56851E-03	2.35828E-03
27	5.00000E+06	1.05332E-06	6.58480E+08	3.66292E-05	7.74972E-05	1.14126E-04
28	1.00000E+07	1.05332E-06	5.45838E+06	2.47540E-07	5.83826E-07	8.31365E-07
29	2.00000E+07	1.05332E-06	1.45921E+04	1.04159E-09	6.23370E-10	1.66496E-09
30	5.00000E+07	1.05332E-06	9.56712E+03	4.86533E-10	4.97655E-10	9.84188E-10

[a]At beginning of timestep 6, all progeny are zero.

TABLE XXI

INTEGRATED ENERGY FROM HALOGENS AND PROGENY IN $^{235}U + n_{th}$ FISSION[a]

Time Step	Cooling Time (s)	MeV		
		Beta	Gamma	Total
6	1.0000E-02	6.4100E-03	9.1279E-03	1.5538E-02
7	1.0000E+00	5.9944E-01	8.7767E-01	1.4771E+00
8	2.0000E+00	1.1677E+00	1.7289E+00	2.8965E+00
9	5.0000E+00	2.7057E+00	4.1411E+00	6.8468E+00
10	1.0000E+01	4.9521E+00	7.8847E+00	1.2837E+01
11	2.0000E+01	8.8050E+00	1.4788E+01	2.3593E+01
12	5.0000E+01	1.8019E+01	3.3202E+01	5.1221E+01
13	1.0000E+02	3.0019E+01	6.0358E+01	9.0377E+01
14	2.0000E+02	4.9108E+01	1.0923E+02	1.5834E+02
15	5.0000E+02	9.5860E+01	2.4313E+02	3.3899E+02
16	1.0000E+03	1.6464E+02	4.5104E+02	6.1568E+02
17	2.0000E+03	2.8913E+02	8.3014E+02	1.1193E+03
18	5.0000E+03	5.9607E+02	1.7438E+03	2.3399E+03
19	1.0000E+04	9.9018E+02	2.8468E+03	3.8369E+03
20	2.0000E+04	1.5899E+03	4.3452E+03	5.9351E+03
21	5.0000E+04	2.8556E+03	6.9707E+03	9.8263E+03
22	1.0000E+05	4.2023E+03	9.3347E+03	1.3537E+04
23	2.0000E+05	5.6461E+03	1.1764E+04	1.7410E+04
24	5.0000E+05	7.5174E+03	1.5159E+04	2.2677E+04
25	1.0000E+06	9.0139E+03	1.8044E+04	2.7058E+04
26	2.0000E+06	1.0334E+04	2.0628E+04	3.0962E+04
27	5.0000E+06	1.0927E+04	2.1833E+04	3.2761E+04
28	1.0000E+07	1.0957E+04	2.1896E+04	3.2853E+04
29	2.0000E+07	1.0957E+04	2.1897E+04	3.2854E+04
30	5.0000E+07	1.0957E+04	2.1897E+04	3.2854E+04

[a]At the beginning of cooling, all progeny are set to zero.

TABLE XXII

NOBLE GASES AND PROGENY VS COOLING TIME FOR $^{235}U + n_{th}$ FISSION[a]

Time Step	Cooling Time (s)	Density	Activity	MeV/Fis Beta	MeV/Fis Gamma	MeV/Fis Total
6	9.99982E-03	2.40330E-05	1.80907E+12	6.23753E-01	5.75725E-01	1.19948E+00
7	1.00000E+00	2.40330E-05	1.75450E+12	5.92543E-01	5.49586E-01	1.14213E+00
8	2.00000E+00	2.40330E-05	1.71608E+12	5.70237E-01	5.32912E-01	1.10315E+00
9	5.00000E+00	2.40330E-05	1.63548E+12	5.22598E-01	5.01787E-01	1.02438E+00
10	1.00000E+01	2.40330E-05	1.55197E+12	4.73718E-01	4.74505E-01	9.48223E-01
11	2.00000E+01	2.40330E-05	1.44730E+12	4.17204E-01	4.41062E-01	8.58266E-01
12	5.00000E+01	2.40330E-05	1.28265E+12	3.38604E-01	3.80600E-01	7.19204E-01
13	1.00000E+02	2.40330E-05	1.15230E+12	2.78178E-01	3.28627E-01	6.06805E-01
14	2.00000E+02	2.40330E-05	1.03016E+12	2.21999E-01	2.81393E-01	5.03392E-01
15	5.00000E+02	2.40330E-05	8.84481E+11	1.63371E-01	2.31562E-01	3.94934E-01
16	1.00000E+03	2.40330E-05	7.93943E+11	1.39173E-01	2.02589E-01	3.41763E-01
17	2.00000E+03	2.40330E-05	7.20405E+11	1.31037E-01	1.74079E-01	3.05116E-01
18	5.00000E+03	2.40330E-05	6.02177E+11	1.05947E-01	1.20081E-01	2.26028E-01
19	1.00000E+04	2.40330E-05	4.94018E+11	7.15245E-02	7.68384E-02	1.48363E-01
20	2.00000E+04	2.40330E-05	3.86849E+11	3.88866E-02	4.18275E-02	8.07141E-02
21	5.00000E+04	2.40330E-05	2.78548E+11	1.30225E-02	1.38577E-02	2.68802E-02
22	1.00000E+05	2.40330E-05	2.29561E+11	7.47804E-03	7.95209E-03	1.54301E-02
23	2.00000E+05	2.40330E-05	1.87881E+11	5.64905E-03	5.83970E-03	1.14888E-02
24	5.00000E+05	2.40330E-05	1.17249E+11	3.64376E-03	3.35091E-03	6.99468E-03
25	1.00000E+06	2.40330E-05	5.48076E+10	1.77335E-03	1.47363E-03	3.24698E-03
26	2.00000E+06	2.40330E-05	1.24682E+10	4.27111E-04	3.17616E-04	7.44727E-04
27	5.00000E+06	2.40330E-05	6.64406E+08	4.61896E-05	4.71058E-06	5.09002E-05
28	1.00000E+07	2.40330E-05	5.14472E+08	4.13922E-05	4.15312E-07	4.18075E-05
29	2.00000E+07	2.40330E-05	5.02299E+08	4.03596E-05	3.67721E-07	4.07274E-05
30	5.00000E+07	2.40330E-05	4.72117E+08	3.79061E-05	3.46106E-07	3.82522E-05

[a]At the beginning of timestep 6, all progeny are zero.

TABLE XXIII

INTEGRATED ENERGY FROM NOBLE GAS AND PROGENY[a]

Time Step	Cooling Time (s)	MeV Beta	MeV Gamma	MeV Total
6	1.0000E-02	6.2413E-03	5.7602E-03	1.2002E-02
7	1.0000E+00	5.9928E-01	5.5521E-01	1.1545E+00
8	2.0000E+00	1.1794E+00	1.0955E+00	2.2750E+00
9	5.0000E+00	2.8071E+00	2.6402E+00	5.4473E+00
10	1.0000E+01	5.2822E+00	5.0726E+00	1.0355E+01
11	2.0000E+01	9.6987E+00	9.6295E+00	1.9328E+01
12	5.0000E+01	2.0818E+01	2.1796E+01	4.2615E+01
13	1.0000E+02	3.6016E+01	3.9347E+01	7.5363E+01
14	2.0000E+02	6.0599E+01	6.9518E+01	1.3012E+02
15	5.0000E+02	1.1664E+02	1.4510E+02	2.6174E+02
16	1.0000E+03	1.9142E+02	2.5265E+02	4.4407E+02
17	2.0000E+03	3.2602E+02	4.3899E+02	7.6501E+02
18	5.0000E+03	6.7452E+02	8.6312E+02	1.5376E+03
19	1.0000E+04	1.1028E+03	1.3351E+03	2.4379E+03
20	2.0000E+04	1.6199E+03	1.8910E+03	3.5109E+03
21	5.0000E+04	2.2728E+03	2.5896E+03	4.8625E+03
22	1.0000E+05	2.7569E+03	3.1046E+03	5.8614E+03
23	2.0000E+05	3.3985E+03	3.7767E+03	7.1752E+03
24	5.0000E+05	4.7257E+03	5.0654E+03	9.7911E+03
25	1.0000E+06	5.9716E+03	6.1553E+03	1.2127E+04
26	2.0000E+06	6.8438E+03	6.8459E+03	1.3690E+04
27	5.0000E+06	7.2804E+03	7.0160E+03	1.4296E+04
28	1.0000E+07	7.4978E+03	7.0238E+03	1.4522E+04
29	2.0000E+07	7.9059E+03	7.0277E+03	1.4934E+04
30	5.0000E+07	9.0740E+03	7.0383E+03	1.6112E+04

[a]At the beginning of cooling, all progeny are set to zero.

flux level was 10^{13} n/cm^2-s. The ratios of the three fast-group fluxes to this value are six, eight, and five, where the latter is the epithermal ratio. The group cross sections were processed from ENDF/B-IV using a typical mid-life PWR spectrum for a weighting function. It should be noted that the thermal (group 4) flux is applied to an effective 2200 m/s cross section defined by

$$\sigma_{eff} = \bar{\sigma}/\bar{\sigma}_{1/v} ,$$

where

$\bar{\sigma}$ = average thermal cross section in the PWR spectrum,

$\bar{\sigma}_{1/v}$ = average of 1/v energy dependent cross section in the PWR spectrum spectrum having a 1 b value at 0.0253 eV. (In the PWR spectrum used here, $\bar{\sigma}_{1/v}$ = 0.55402 b.)

Therefore, the 10^{13} n/cm^2-s should be interpreted as a neutron density, and the calculated group 4 aggregate cross section is an effective 2200 m/s value. Similarly, the corresponding group flux ratios are, in effect, equivalent to a reduction by the factor $\bar{\sigma}_{1/v}$.

In these tables, the first five time steps are of equal duration (1728 h) and are at power (100 W/cm^3). The remaining time steps follow shutdown and extend out to 5 x 10^7 s. Tables XV-XIX include all fission products. Tables XX and XXI include only halogens and those progeny generated after shutdown (following time step 5). Tables XXII and XXIII include only noble gases and those progeny generated after shutdown. While the first five tables are based on all fission products, Tables XX-XXIII include only gases and their progeny, which are built up from decay following shutdown. Where actual values, rather than fractions, are listed all results are given per cm^3. The constant fission rate prior to shutdown uses a nominal 200 MeV/fission to produce a power of 100 watts.

One interesting result noted in the last progress report and even more pronounced for short irradiation times is the fraction of energy due to noble gases and halogens (Table XVII). At 5000 s cooling 13.2% of the products are gases but only 0.6% are radioactive gases, yet these account for 21% of the activity, 16% of the beta energy rate, 35% of the gamma energy rate, and 27% of the total energy release rate. Of the 78 radioactive gases at 5000 s cooling, 6 contribute 1% or more of the beta, gamma, or total energy release rate -- ^{87}Kr, ^{88}Kr, ^{131}Xe,

^{133}I, ^{134}I, and ^{135}Xe. (Tabular results for individual nuclides are too extensive for inclusion in this report.)

E. CINDER-10 Code Development (T. R. Fngland, N. L. Whittemore, and W. B. Wilson)

Improvements were made which reduced the charge per run by approximately a factor of ten. Other algorithms and edits were added to produce information requested by the Nuclear Regulatory Commission.

Normally CINDER-10 calculations use LASL's CDC 6600 (Machine 0) because of the large storage required for the ENDF/B-IV library. An untested version is operational on the CDC 7600 using LCM. Other work is in progress to reduce the required storage.

F. Beta-Energy Averaging and Beta Spectra (M. G. Stamatelatos and T. R. England)

A simple, efficient, and highly accurate method for approximately calculating spectrum-averaged beta energies and beta spectra for radioactive nuclei was developed and partially discussed in the last progress report. The final version will be published as LASL report LA-6445-MS (ENDF-242).

G. Absorption Buildup Studies (W. B. Wilson, T. R. England, M. J. Stamatelatos, and R. J. LaBauve)

A new fission-product absorption data set for a revised version of the CINDER[71] code has been completed using ENDF/B-IV decay constants, branching fractions, fission yields, and processed neutron radiative capture cross sections. The details of procedure and codes used in the data processing have been described previously.[72] The data set describes the temporal coupling of 186 fission product nuclei using 84 linearized nuclide chains and a total of 484 linearized nuclides. Each chain describes a unique path via neutron absorption and radioactive decay.

A reduced 12-chain data set has also been completed, describing 27 principal fisson-product nuclei with 11 chains and 34 linearized nuclides. The balance of neutron-absorption accumulation is described in a single, non-saturating chain of 4 pseudo-fission product nuclei.

Macroscopic absorption calculations for a typical reactor lifetime with the two data sets differ by less than 1%. These quantities vary less than 2% even after an additional equivalent period of decay.

In contrast to the data libraries and code version used to produce results in previous sections of this report, these libraries are intended for use only in absorption buildup studies, including transients, in reactor design. The 12-chain set is suitable for spatial depletion codes, and the 84-chain set, in addition to its use in parameterizing the pseudo-chain, is useful in providing the inventories of nuclides having half-lives longer than ~4 hours. The 4-group cross sections used in these libraries were collapsed from a 154-multigroup set described in the previous progress report.

REFERENCES

1. R. Brown, Los Alamos Scientific Laboratory, private communication (1976).

2. C. M. Bartle, "A Study of the $^{6}Li(n,\alpha)T$ Reaction Between 2-10 MeV," Nuclear Cross Sections and Technology Conference Proceedings NBS Special Publication 425, Vol. II, p. 688 (1975) and private communication (1976)

3. P. J. Clements and I. C. Rickard, Atomic Energy Research Establishment report AERE-R-7075 (1972).

4. R. A. Schrack, O. A. Wasson, and G. P. Lamaze, " A Measurement of the $^{10}B(n,\alpha\gamma)\ ^{7}Li$ Cross Section in the keV Energy Region," Bull. Am. Phys. Soc. 21, 513 (1976) and private communication (1976).

5. V. Konig, W. Gruebler, R. E. White, P. A. Schmelzbach, and P. Marmier, "Measurement of the Analyzing Powers iT_{11}, T_{20}, T_{21}, and T_{22} in d-^{3}He Elastic Scattering," Nucl. Phys. A185, 263 (1972).

6. B. Jenny, W. Gruebler, V. Konig, P. A. Schmelzbach, R. Risler, D. O. Boerma, and W. G. Weitkamp, "Measurement of the Analyzing Powers in $^{3}He(d,d)^{3}He$ Scattering," Proc. Fourth International Symposium in Nuclear Reactions, Zurich (1975) and private communication (1976).

7. W. Klinger, F. Dusch, and R. Fleischmann, "The Analyzing Power of the Reaction $^{3}He(d,p)^{4}He$ for Vector-Polarized Deuterons Between 2 and 13," Nucl. Phys. A166, 253 (1971).

8. D. Fick, private communication (1976).

9. M. Drosg, private communcation (1976).

10. L. R. Veeser and E. D. Arthur, "Measurement of (n,2n) and (n,3n) Cross Sections," Bull. Am. Phys. Soc. 20, 1191 (1975).

11. J. Frehaut and G. Mosinski, "Measurement of (n,2n) and (n,3n) Cross Sections for Incident Energies Between 6 and 15 MeV," Nuclear Cross Sections & Technology Conference Proceedings NBS Special Publication 425, p. 855 (1975).

12. B. P. Bayhurst, J. S. Gilmore, R. J. Prestwood, J. B. Wilhelmy, Nelson Jarmie, B. H. Erkkila, and R. A. Hardekopf, "Cross Sections for (n,xn) Reactions Between 7.5 and 28 MeV," Phys. Rev. C12, 451 (1975).

13. G. M. Braga-Marcazzan, E. Gadioli-Erba, L. Milazzo-Colli, and P. G. Sona, "Analysis of Total (n,p) Cross Sections Around 14 MeV with the Pre-equilibrium Excitation Model," Phys. Rev. C6, 1398 (1972).

14. C. Kalbach-Cline, "Residual Two-Body Matrix Elements for Preequilibrium Calculations," Nucl. Phys. A210, 590 (1973).

15. S. M. Grimes, R. C. Haight, and J. D. Anderson, "Observations of Sub-Coulomb Barrier Protons from 14 MeV Neutron Bombardment of Al and Ti," Bull. Am. Phys. Soc. 21, 663 (1976).

16. L. Milazzo-Colli and G. M. Braga-Marcazzan, "α-Emission by Pre-Equilibrium Processes in (h,α) Reactions," Nucl. Phys. A210, 297 (1973).

17. P. G. Young, Ed., "Applied Nuclear Data Research and Development Quarterly Progress Report," Los Alamos Scientific Laboratory report LA-6018-PR, p.3, (1975).

18. D. W. Muir and P. G. Young, Eds., "Applied Nuclear Data Research and Development Quarterly Progress Report," Los Alamos Scientific Laboratory report LA-6123-PR, p. 3 (1975).

19. P. C. Fisher and L. B. Engle, "Delayed Gammas from Fast-Neutron Fission of ^{232}Th, ^{233}U, ^{235}U, ^{238}U, and ^{239}Pu," Phys. Rev. B134, 796 (1964).

20. D. R. Harris, D. E. Dei, A. A. Husseiny, Z. A. Sabri, and G. M. Hale, "The STEEP4 Code for Computation of Specific Thermonuclear Reaction Rates from Pointwise Cross Sections," Los Alamos Scientific Laboratory report LA-6344-MS (1976).

21. J. M. Dawson, H. P. Furth, and F. H. Tenny, "Production of Thermonuclear Power by Non-Maxwellian Ions in a Closed Magnetic Field Configuration," Phys. Rev. Lett. 26, 1156 (1971).

22. G. M. Hale, R. A. Nisley, and D. C. Dodder, Los Alamos Scientific Laboratory, private communication (1975).

23. G. Hale, D. R. Harris, and P. G. Young, "The $^{11}B(p,\alpha)^{8}Be$ Cross Section and Specific Reaction Rate," in "Applied Nuclear Data Research and Development Quarterly Progress Report, Los Alamos Scientific Laboratory report LA-5546-PR p.6 (1974).

24. S. L. Greene, Jr., "Maxwell Averaged Cross Sections for Some Thermonuclear Reactions on Light Isotopes," University of California Radiation Laboratory report UCRL-70522 (1967).

25. B. H. Duane, "Fusion Cross Section Theory," in "The Pacific Northwest Laboratory Annual Report on Controlled Thermonuclear Reactor Technology - 1972," Battelle Northwest Laboratory report BNWL-1685 p. 75 (1972).

26. G. H. Miley, H. Towner, and N. Ivich, "Fusion Cross Sections and Reactivities," University of Illinois at Urbana-Champaign report COO-2218-17 (1974).

27. C. Bathke, H. Towner, and G. H. Miley, "Fusion Power by Non-Maxwellian Ions in D-T, D-D, D-^{3}He, and p-^{11}B Systems, Trans. Am. Nucl. Soc. 17, 41 (1973).

28. R. B. Kidman, Los Alamos Scientific Laboratory, private communication (1976).

29. K. D. Lathrop, "GAMLEG - A FORTRAN Code to Produce Multigroup Cross Sections for Photon Transport Calculations," Los Alamos Scientific Laboratory report LA-3267 (1965).

30. R. E. Seamon, Los Alamos Scientific Laboratory, private communication (1976).

31. Leona Stewart and Phillip G. Young, "Evaluated Nuclear Data for CTR Applications," Trans. Am. Nucl. Soc. 23, 22 (1976).

32. R. J. LaBauve, C. R. Wesibin, R. E. Seamon, M. E. Battat, D. R. Harris, P. G. Young, and M. M. Klein, "PENDF: A Library of Nuclear Data for Monte Carlo Calculations Derived from Data in the ENDF/B Format," Los Alamos Scientific Laboratory report LA-5687 (October 1974).

33. C. R. Wesibin, P. D. Soran, R. E. MacFarlane, D. R. Harris, R. J. LaBauve, J. S. Hendricks, J. E. White, and R. B. Kidman, "MINX, A Multigroup Interpretation of Nuclear X-Sections from ENDF/B," Los Alamos Scientific Laboratory report LA-6486-MS (to be published).

34. D. Garber, Ed., "Data Formats and Procedures for the ENDF Neutron Cross Section Library," Brookhaven National Laboratory report BNL-50274 (1976).

35. R. W. Hardie and W. W. Little, Jr., "1DX A One-Dimensional Diffusion Code for Generating Effective Nuclear Cross Sections," Battelle Northwest Laboratory report BNWL-954 (March 1969).

36. H. Henryson, II and B. J. Toppel, "MC^{2}-2: A Code to Calculate Fast Neutron Spectra and Multigroup Cross-Sections," Argonne National Laboratory report ANL-8144 (to be published).

37. R. W. Hardie, R. E. Schenter, and R. E. Wilson, "An Analysis of Selected Fast Critical Assemblies Using ENDF/B-IV," Nucl. Sci. and Eng. 57, 3 (1975).

38. R. B. Kidman and R. E. MacFarlane, "LIB-IV, A Library of Group Constants for Nuclear Reactor Calculations," Los Alamos Scientific Laboratory report LA-6260-MS (March 1976).

39. B. M. Carmichael, "Standard Interface Files and Procedures for Reactor Physics Codes, Version III," Los Alamos Scientific Laboratory report LA-5486-MS (1974).

40. R. B. Kidman and R. E. MacFarlane, "CINX: Collapsed Interpretation of Nuclear X-Sections," Los Alamos Scientific Laboratory report LA-6287-MS, (April 1976).

41. EPRI-CELL is a proprietary product of the Nuclear Associates International Corp., 6003 Executive Blvd., Rockville, Maryland. See also, W. J. Eich, "Advanced Recycle Methodology Program Project Status Report," Electric Power Research Institute report EPRI-118-1 (December 1975).

42. H. C. Honeck, "THERMOS, A Thermalization Transport Theory Code for Reactor Lattice Calculations," Brookhaven National Laboratory report BNL-5826 (1961).

43. G. D. Joanon and J. S. Dudek, "GAM-I, A Consistent P_1 Multigroup Code for the Calculation of Fast Neutron Spectra and Multigroup Constants," General Atomic report GA-1850 (1961).

44. J. R. Askerv, F. J. Fayers, P. B. Kemshell, "A General Description of the Lattice Code WIMS," J. Brit. Nucl. Soc. 5, 564 (1966).

45. C. Wong, J. D. Anderson, P. Brown, L. F. Hansen, J. L. Kammerdiener, C. Logan, and B. Pohl, "Livermore Pulsed Sphere Program: Program Summary through July 1971," Lawrence Livermore Laboratory report UCRL-51144, Rev. 1 (February 1972).

46. E. F. Plechaty and R. J. Howerton, "Calculational Models for LLL Pulsed Spheres," Lawrence Livermore Laboratory report UCID-16372 (1973).

47. C. Wong, private communication (April 1976).

48. K. D. Lathrop, "DTF-IV, A FORTRAN-IV Program for Solving the Multigroup Transport Equation with Anisotropic Scattering," Los Alamos Scientific Laboratory report LA-3373 (November 1965).

49. R. E. MacFarlane and R. M. Boicourt, "NJOY: A Neutron and Photon Cross-Section Processing System," Trans. Am. Nucl. Soc. 22, 720 (1975).

50. E. D. Cashwell, J. R. Neergaard, W. M. Taylor, and G. D. Turner, "MCN: A Neutron Monte Carlo Code," Los Alamos Scientific Laboratory report LA-4751 (January 1972).

51. R. J. Howerton, "Testing of ENDF/B-IV Evaluations with SDT-10 Benchmark Pulsed Spheres," Lawrence Livermore Laboratory report UCRL-75693 (May 1974).

52. T. R. England and R. E. Schenter, "ENDF/B-IV Fission-Product Files: Summary of Major Nuclide Data," Los Alamos Scientific Laboratory report LA-6116-MS (ENDF-223) (October 1975).

53. M. E. Meek and B. F. Rider, "Compilation of Fission Product Yields, Vallecitos Nuclear Center, 1974," General Electric Company report NEDO-12154-1, 74NED6 (January 1974).

54. J. O. Rasmussen, W. Norenberg, and H. J. Mang, "A Model for Calculating the Angular Momentum Distribution of Fission Fragments," Nucl. Phys. A136 465 (1969).

55. Robert Vandenbosch and John R. Huizenga, Nuclear Fission (Academic Press, New York, 1973) p. 369.

56. Kurt Wolfsberg, "Estimated Values of Fractional Yields from Low Energy Fission and a Compilation of Measured Fractional Yields," Los Alamos Scientific Laboratory report LA-5553-MS (May 1974).

57. C. Rudy, R. Vandenbosch, and C. T. Radcliffe, "Relative Independent Yields for ^{95}Nb and ^{95m}Nb from Low Energy Fission," J. Inorg. Nucl. Chem. 30, 365 (1968).

58. H. Warhanek and R. Vandenbosch, "Relative Cross-Sections for Formation of the Shielded Isomeric Pair ^{134m}Cs and ^{134}Cs in Medium Energy Fission," J. Inorg. Nucl. Chem. 26, 669 (1964).

59. I. F. Croall and H. H. Willis, "The Yields of the Isomers of ^{81}Se and ^{83}Se in the Thermal Neutron Fission of ^{239}Pu," J. Inorg. Nucl. Chem. 25, 1213 (1963).

60. S. Amiel and H. Feldstein, "A Systematic Odd-Even Effect in the Distribution of Nuclides from Thermal-Neutron-Induced Fission of ^{235}U," Proceedings of the Third Intern. Atomic Energy Agency Symposium on Physics and Chemistry of Fission, Rochester, New York, 1973 (International Atomic Energy Agency, Vienna, Austria, 1974) Vol. II, p. 65.

61. S. Amiel and H. Feldstein, "Odd-Even Systematics in Neutron Fission Yields of ^{233}U and ^{235}U," Phys. Rev. C11, 845 (1975).

62. E. A. C. Crouch, "Assessment of Known Indepedent Yields and the Calculation of Those Unknown in the Fission of ^{232}Th, ^{233}U, ^{238}U, ^{239}Pu, ^{240}Pu, and ^{241}Pu," Atomic Energy Research Establishment report AERE-R-7680 (May 1974).

63. A. R. deL. Musgrove, J. L. Cook, and C. D. Trimble, "Prediction of Unmeasured Fission Product Yields," in Proceedings of International Atomic Energy Agency Fission Product Nuclear Data Panel, Bologna, Italy, 1973 (International Atomic Energy Agency, Vienna, Austria 1974) Vol. II, p. 163.

64. Kurt Wolfsberg, "Estimated Values of Fractional Yields from Low Energy Fission," Los Alamos Scientific Laboratory report LA-5553-MS (May 1974).

65. H. C. Britt, M. Bolsterli, J. R. Nix, and J. L. Norton, "Fission Barriers Deduced from the Analysis of Fission Isomer Results," Phys. Rev. C9, 1924, (1974).

66. B. B. Black, Ole Hansen, H. C. Britt, and J. D. Garrett, "Fission of Doubly Even Actinide Nuclei Induced by Direct Reactions," Phys. Rev. C9, 1924 (1974).

67. B. B. Black, H. C. Britt, Ole Hansen, B. Leroux, and J. D. Garrett, "Fission of Odd-A and Doubly Odd Actinide Nuclei Induced by Direct Reactions," Phys. Rev. C10, 1948 (1974).

68. D. G. Madland and T. R. England, "The Influence of Pairing on the Distribution of Independent Yield Strengths in Neutron-Induced Fission," Los Alamos Scientific Laboratory report LA-6430-MS (ENDF-240) (1976).

69. P. A. Seeger and W. M. Howard, "Table of Calculated Nuclear Properties," Los Alamos Scientific Laboratory report LA-5750 (October 1974).

70. N. Tsoulfanidis, B. W. Wehring, and M. E. Wyman, "Measurements of Time-Dependent Energy Spectra of Beta Rays from Uranium-235 Fission Fragments," Nucl. Sci. and Eng. 43, 42 (1971).

71. T. R. England and R. E. Schenter, "ENDF/B-IV Fission-Product Files: Summary of Major Nuclear Data," Los Alamos Scientific Laboratory report LA-6116-MS (ENDF-223) (October 1975).

72. C. I. Baxman, G. M. Hale, and P. G. Young, Compilers, "Applied Nuclear Data Research and Development Quarterly Progress Report for the period January 1 through March 31, 1976," Los Alamos Scientific Laboratory report LA-6472-PR (1976).

☆ U.S. GOVERNMENT PRINTING OFFICE. 1976—777-018/16